energies

MDPI

Review

Nanoparticle-Enhanced Phase Change Materials (NPCMs) in Solar Thermal Energy Systems: A Review on Synthesis, Performance, and Future Prospects

Wei Lu [1,2], Jay Wang [1,*], Meng Wang [3], Jian Yan [4], Ding Mao [5] and Eric Hu [6]

[1] School of Engineering, Computer & Mathematical Sciences, Auckland University of Technology (AUT), Auckland 1010, New Zealand; lw0426@outlook.com
[2] Guangdong Provincial Mechanical Engineering Experimental Teaching Center, Guangdong Technology College, Zhaoqing 266041, China
[3] Department of Energy and Power Engineering, Tsinghua University, Beijing 100190, China; meng-wang@mail.tsinghua.edu.cn
[4] College of Mechanical Engineering, Hunan University of Science and Technology, Xiangtan 411201, China; yanjian1988@hnust.edu.cn
[5] Department of Building Environment and Equipment, School of Civil Engineering, Hefei University of Technology, Hefei 230002, China; maoding@hfut.edu.cn
[6] School of Electrical and Mechanical Engineering, The University of Adelaide, Adelaide, SA 5000, Australia; eric.hu@adelaide.edu.au
* Correspondence: jay.wang@aut.ac.nz; Tel.: +64-9-921-9001 (ext. 33206)

Abstract

The environmental challenges posed by global warming have significantly increased the global pursuit of renewable and clean energy sources. Among these, solar energy stands out due to its abundance, renewability, low environmental impact, and favorable long-term economic viability. However, its intermittent nature and dependence on weather conditions hinder consistent and efficient utilization. To address these limitations, nanoparticle-enhanced phase change materials (NPCMs) have emerged as a promising solution for enhancing thermal energy storage in solar thermal systems. NPCMs incorporate superior-performance nanoparticles within traditional phase change material matrices, resulting in improved thermal conductivity, energy storage density, and phase change efficiency. This review systematically examines the recent advances in NPCMs for solar energy applications, covering their classification, structural characteristics, advantages, and limitations. It also explores in-depth analytical approaches, including mechanism-oriented analysis, simulation-based modelling, and algorithm-driven optimization, that explain the behavior of NPCMs at micro and macro scales. Furthermore, the techno-economic implications of NPCM integration are evaluated, with particular attention to cost-benefit analysis, policy incentives, and market growth potential, which collectively support broader adoption. Overall, the findings highlight NPCMs as a frontier in materials innovation and enabling technology for achieving low-carbon, environmentally responsible energy solutions, contributing significantly to global sustainable development goals.

Keywords: phase change material; solar energy; nanoparticle-enhanced; NPCM

Academic Editors: Carlos Miguel Costa and Ziad Saghir

Received: 17 June 2025
Revised: 18 July 2025
Accepted: 21 August 2025
Published: 25 August 2025

Citation: Lu, W.; Wang, J.; Wang, M.; Yan, J.; Mao, D.; Hu, E. Nanoparticle-Enhanced Phase Change Materials (NPCMs) in Solar Thermal Energy Systems: A Review on Synthesis, Performance, and Future Prospects. *Energies* **2025**, *18*, 4516. https://doi.org/10.3390/en18174516

1. Introduction

Traditional fossil fuel combustion releases substantial carbon dioxide emissions, constituting the dominant source of greenhouse gases. These emissions drive global warming, ecosystem disruptions [1], and extreme weather events [2]. Simultaneously, in accordance

with the 2024 United Nations World Population Prospects, the global population is projected to reach 10.1 billion by 2061 and continue its growth trajectory, which directly causes a relentless increase in energy demand [3]. Due to the dual pressures of rapid population growth and surging energy demands, the adoption of abundant, clean, and eco-friendly renewable energy has become imperative.

Solar energy, which possesses notable advantages in terms of its environmental friendliness, abundant supply, and high degree of independence, has been widely used in energy systems such as photovoltaic (PV) power generation [4], solar thermal conversion [5,6], solar cooling [7,8], and solar still [9], thereby offering tremendous potential for sustainable energy systems. In the domain of solar energy utilization, the intermittent and non-stable nature of solar energy poses significant challenges, so high-efficiency heat storage technology has emerged as a pivotal breakthrough for enhancing the utilization efficiency of solar energy [10]. In solar energy systems, solar radiant energy is first converted into thermal energy via heat collection devices, so heat storage technology becomes essential for the spatio-temporal transfer and stable output of this energy [11,12]. Among various heat storage strategies, the latent heat storage technology founded upon phase change material (PCM) has set itself apart due to its distinctive operational mechanism [13,14]. The PCM materials listed in Table 1 were selected for comparison due to their diverse chemical structures (paraffins, salt hydrates, and eutectic mixtures), varied phase change temperatures, and widespread use in thermal storage. This selection enables the systematic evaluation of nanoparticle (NP) dispersion effects on key PCM parameters, such as thermal conductivity and latent heat.

Table 1. Properties of some PCM.

PCM	Density of Solids	Density of Liquids	Specific Heat Capacity	Latent Heat	Thermal Conductivity (TC)	Temp. of Solids	Temp. of Liquids	Melting Temp. Range	Ref.
Unit	**kg/m^3**	**kg/m^3**	**J/(kg·K)**	**kJ/kg**	**W/(m·K)**	**°C**	**°C**	**°C**	
RT28	880	770	2000	179	0.2	25.98	29.6	3.63	[15]
RT28HC	-	-	2000	250	0.2	27	28	-	[16]
RT35	860	-	2000	182	0.3	-	-	1.5	[17]
RT42	880	760	2000	165	0.2	-	-	4	[18]
RT50	876	710	2100	160	0.2	-	-	7	[19]
RT55	880	770	2000	170	0.2			6	[20]
RT58	840	-	2100	180	0.2	321	335		[21]
60% $NaNO_3$ + 40% KNO_3	1980	-	1575	140	0.59	495	519	-	[22]
53% $NaNO_3$ + 40%KNO_3 + 7%$NaNO_2$	1800 at 400 °C	-	1500 at 400 °C	-	-	-	-	-	[23]
KNO_3	2109	-	953	95	0.5	-	-	-	[24]
Dodecyl sulfate	-	-	-	200	-	-	-	-	[25]
Lauric acid	940	885	2285	-	0.15	40.48	42.48	2	[26]
HS 29	1681	1530	1510 (S) 2620 (L)	190	0.382 (L) 0.478 (S)	-	-	-	[27]
Coconut Oil	-	-	2350 (S) 3230 (L)	70–100	-	-	-	-	[28]
Eicosane	810	770	1900 (S) 2200 (L)	241	0.4 (S) 0.157 (L)	-	-	-	[29]
$C_{28}H_{58}$	-	806	-	254	-	-	-	-	[30]

The incorporation of high-performance nanoparticles, such as Cu for reducing melting time, Al_2O_3 for accelerating solidification, and graphite for enhancing thermal conductivity (TC), into phase change materials to form nanocomposite phase change materials can sig-

nificantly improve solar energy conversion efficiency and thermal storage capacity [31,32]. Their core advantages are mainly reflected in the following aspects. The high heat storage density enables the efficient accumulation of thermal energy within confined spaces, thereby maximizing the utilization of available volume [33,34]. The isothermal behavior during the phase change process ensures the thermal stability of the heat storage system, which is crucial for solar-thermal applications that require a consistent heat source [35,36]. Meanwhile, the minimal phase change temperature difference significantly mitigates heat losses during the heat storage cycle, leading to enhanced energy utilization efficiency [37].

Based on the analysis above, NPCM materials have been widely and intensively studied and analyzed in the scientific research community. However, the research gaps lie in the lack of a review paper that summarizes the latest applications of NPCM in high-temperature thermal energy storage systems, particularly in terms of energy performance through mechanism analysis, simulation, and algorithm. Therefore, the general aim of this review article is to systematically introduce various research and analysis methods from the perspective of NPCM models.

This review is primarily divided into six sections. Section 1 covers the latest developments in NPCMs reported in recent literature. Section 2 focuses on introducing various structural characteristics of NPCMs. Section 3 concentrates on the mechanisms and simulation analysis methods of NPCMs, spanning from the material's microscopic structure to its comprehensive applications. Section 4 demonstrates the algorithm-driven optimization of NPCMs, including machine learning methods and uncertainty analysis. Section 5 discusses techno-economic analysis, including cost-benefit analysis, and policy incentives. Finally, the conclusions and future research directions in the field of NPCMs are proposed in Section 6.

2. Nano-Enhanced Phase Change Material (NPCM)

NPCM has high heat storage density for efficient limited space energy storage, isothermal phase change thermal stability, and a minimal phase—change temperature difference that cuts heat storage cycle losses. These unique properties give PCM-based latent heat storage technology extensive application potential across a wide range of fields, including solar thermal power generation, building energy-efficiency improvements, and electronic thermal management. As such, it represents a crucial technological pathway for addressing the intermittent issue of solar energy and facilitating the efficient utilization of renewable energy resources. From a structural perspective, NPCM can be classified based on the configuration of the nanomaterial within the composite: thermophysical NPCM (dispersed NPs), photonic NPCM (NPs with light-responsive surfaces), NPCM fluids (NP suspensions), nano-encapsulated PCM (core-shell nanostructures), and phase-engineered nanomaterials (NPs with designed phase interfaces).

2.1. Thermophysical NPCM

Thermophysical NPCM enhances PCM properties by incorporating nanoparticles (NPs) like graphene and metal compounds, which strengthen thermal conductivity [38]. Abdolahimoghadam designed a bio-based NPCM composed of coconut oil, beeswax, and graphene-Cu hybrid NPs. Research shows that the addition of graphene nanosheets (GNP) to the material can significantly increase the melting rate by 5.05% [39]. Gopi selected bismuth oxychloride, CuO, and their mixture (composite) as NPs and stearic acid as the PCM. They found that the latent heats of NPCMs containing 0.5 wt% bismuth oxychloride, CuO, and the composite were 204.6 $kJ \cdot kg^{-1}$, 198.3 $kJ \cdot kg^{-1}$, and 201.7 $kJ \cdot kg^{-1}$, respectively, and the thermal conductivities increased to 0.19 $W/(m \cdot °C)$, 0.22 $W/(m \cdot °C)$, and 0.20 $W/(m \cdot °C)$, respectively, which were 5.9%, 29.4%, and 17.6% higher than those of the pure PCM [40].

2.2. Photonic NPCM

Photonic NPCM enhances photovoltaic-thermal system performance when combined with nanofluids, improving light absorption [41]. Ahmed used 0.6% silicon carbide-enhanced nanofluid and silicon carbide to enhance the PCM in photovoltaic systems, thereby improving the photovoltaic-thermal efficiency. The research results show that the maximum energy power increased from 17.512 W to 26 W [42]. Under the working conditions of 47.94 °C and a flow rate of 5 L/min, Maseer studied a semi-circular absorber-tube-type solar photovoltaic-thermal (PVT) system with combined cooling of nanofluid and NPCM. The research results of this study show that the power-generation efficiency was 12.70%, the heat generation efficiency was 78.99%, and the total efficiency was 91.83% [43]. Máñez has developed a simple yet effective reconfigurable all-dielectric metasurface design that enables full control of the electromagnetic response, including electrical, magnetic, and electromagnetic coupling, by changing the refractive index of the PCM layer [44].

2.3. NPCM Fluids

NPCM fluids are liquid-phase composite materials formed by dispersing NPs, particularly molten salt compounds, within PCM or base fluids, demonstrating superior specific heat capacity. Sathishkumar formed NPCM clusters by using the fatty-acid-based PCM OM05 and a GNP suspension, which led to research results showing that for the Oleic-acid-modified (OM) 05-based NPCM with 0.75 wt% GNP, its TC increased significantly at 30 °C, the total solidification time was shortened by 32%, and as a result, a more efficient cooling and charging rate was achieved (Shown in Figure 1) [45]. Baiju devised a conical-fin latent heat storage system utilizing HS-89 hydrated salt as the matrix, incorporating 0.5 wt% graphene nanoplatelets (GNP) and 0.5 wt% nano-alumina (nAl_2O_3), achieving a 56% reduction in charging time [46]. Wu added 5 wt% of OM and nanoAl (3:1) to binary alkanes, which caused TC to increase to 0.31 W/(m·K) and the melting time to decrease by 38.3% [47].

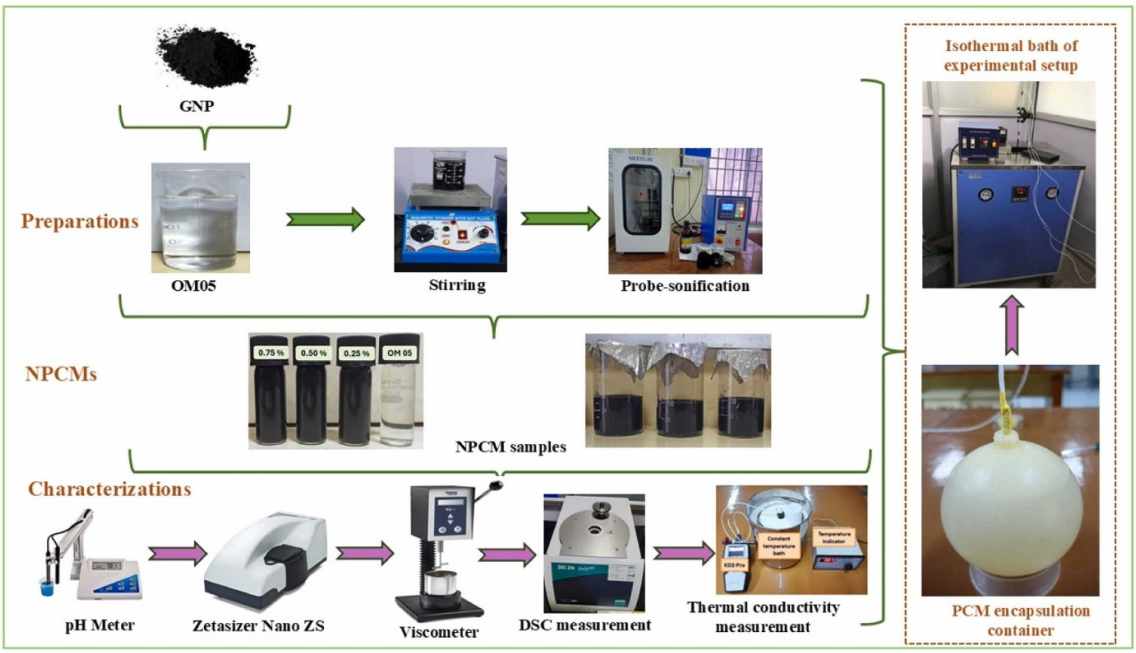

Figure 1. The preparation process of the OM05-based NPCM. (Reproduced with permission from [45], Elsevier, 2025).

2.4. Encapsulated NPCM

Encapsulated NPCM is a composite PCM that combines NPs or nanomaterials with PCM, which can effectively prevent liquid leakage during equipment operation. Shijina added the developed GNE-PCM to an ethylene-glycol-water mixture to prepare a graphene nano-encapsulated composite material, and the research showed that TC, specific heat capacity, and cooling efficiency of the material were all improved [48]. To study the effect of GNP on the thermal properties of NPCM for encapsulated heat sinks, Sivashankar added different concentrations of GNP to the OM35 base to prepare NPCM. The research results showed that 0.5 vol% of GNP led to a significant increase in both TC and thermal diffusivity of NPCM [49]. Sutheesh encapsulated tetradecan-1-ol with polymethyl methacrylate to form NPCM for thermal regulation of Lithium-ion Battery (LIB). The research results showed that for LIB with added NPCM, heat generation was reduced, and both the convective heat transfer coefficient and the discharge rate were improved [50].

2.5. Phase-Engineered Nanomaterials

Phase-Engineered Nanomaterials refer to the optimization of the physical and chemical properties of materials themselves by designing the crystal-phase structure of nanomaterials [51,52]. Liu used palladium-selenide as a model system, which was then transformed into $Pd_{17}Se_{15}$ and Pd_4Se phases by thermally regulating the component ratio. Through precise control of the electrode thickness and spacing, different phase-configuration arrangements could be obtained, which enabled multiple in-situ functions and extended to 29 elemental combinations between metals and chalcogens, as reported in reference [53]. Zang developed an amorphous-crystalline CuxS–Ag_2S composite with a significant temperature gradient, which achieved a synergistic enhancement of optimal thermoelectric therapy and multi-enzyme activity, as indicated in reference [54]. Yang developed a bismuth-doped ruthenium oxide single-atom alloy oxide catalyst, which achieved a current density of 1.0 A cm^{-2} at only 1.59 V under industrial conditions, according to reference [55]. Some NPCM performance improvements are listed in Table 2.

Table 2. Properties of some NPCM.

Reference	Materials Set-Up	Analysis of Performance Improvement
Abdolahimoghadam et al. [39]	Graphene-Cu NPs are added to the bio-nano-based materials of coconut oil and beeswax.	The melting time of the four-tube system with 2 wt% Graphene-Cu hybrid NPs added is shortened by 80.25%, and the solidification time is shortened by 74.28%.
Kannan et al. [40]	CuO NPs are added to stearic acid.	The enhanced TC of NPCM with 0.5 wt% CuO NPs is 29.4% higher than that of pure PCM, and the congruent melting rate is increased by 31%.
Ahmed et al. [42]	SiC NPs are added to water to prepare nanofluids, and SiC NPs are added to paraffin to prepare NPCM.	When nanofluid with 0.6 vol% and NPCM with 1 vol% are added to the collector, the thermal efficiency improves by 86.2%, the electrical energy increases by 11.24%, and the maximum photovoltaic power output grows from 17.512 W to 26 W.
Maseer et al. [43]	0.1% of Al_2O_3 NPs are introduced into water to prepare nanofluids. Subsequently, 0.65% of paraffin is introduced into the nanofluids to prepare NPCM.	The PVT system with NPCM coolant achieves a maximum power of 73.25 W, with a thermal efficiency of 70.5%, an electrical efficiency of 16.9% and a maximum overall efficiency of 84.23%.
Máñez-Espina et al. [44]	Ge, Ge2Sb2Te5, CaF_2	Energy coupling efficiency, energy efficiency, and unidirectional absorption asymmetry can all be improved.
Sathishkumar et al. [45]	0.75% of GNP is added to OM to prepare NPCM.	TC of the cold-heat energy storage system has been significantly increased by 54%, and the total freezing time has been significantly reduced by 32%.
Baiju et al. [46]	Hydrated salt is prepared with 0.5 wt% GNP and 0.5 wt% nano-Al.	The charging time of the latent heat storage device that uses conical fins and NPCM in combination is shortened by 56%, and the annual life-cycle cost is 162.3 euros per year.
Wu et al. [47]	Binary alkane containing 5 wt% modified nano-Al_2O_3.	TC of NPCM with 5 wt% modified NPs is 0.31 W/m·K, and the melting time is reduced by 38.3%.

Table 2. *Cont.*

Reference	Materials Set-Up	Analysis of Performance Improvement
Shijina et al. [48]	Graphene flakes are affixed to polystyrene spherical balls encapsulated with a composite PCM of 80% paraffin and 20% octadecane, and then these are dispersed in an ethylene-glycol-water mixture to obtain nanofluid.	The subcooling degree of the coolant is reduced by 50%, and TC and viscosity of the nanofluid increase by 14.7% and 19%, respectively, and the heat capacity is increased by 56.7%.
Sivashankar et al. [49]	Organic PCM is prepared with 0.5 vol% GNP and OM35.	TC of the solid phase has increased by 93%, the conductivity of the liquid phase has increased by 78%, the thermal diffusivity of the solid phase has increased by 119%, the thermal diffusivity of the liquid phase has increased by 124%, the starting temperature has decreased to 31.21 °C, the peak temperature has decreased to 37.46 °C, the viscosity has increased by 76%, and the latent heat has increased by 19.82%.
Sutheesh et al. [50]	Tetradecan-1-ol serves as the PCM, while deionized water acts as the base fluid. The shell is constituted by polymethyl methacrylate, and MgO functions as the filling material.	The lowest Reynolds number during the highest cell discharge optimizes the phase transition of PCM. When the Reynolds number is 121.09 and the discharge rate is 5C, the convective HTC increases by 4.53 times and 6.15 times for 1% and 4% NPCM, respectively.
Liu et al. [53]	Pd–Se	Through regulating the thickness and the distance between electrodes on the apparatus, we bring about emerging phases. These phases display superconducting orders or can be manipulated to produce an ultralow resistance contact for 2D semiconductor transistors. Additionally, the phase engineering carried out on-device enables in-situ and customized synthesis of outstanding electrocatalysts, which has the ability to surpass the traditional modulation limit of composition proportion.
Zang et al. [54]	Cu_xS-Ag	Abundant active sites are furnished for improving the therapeutic activity by the dangling bonds on the amorphous Cu_xS surface. Moreover, through non-radiative relaxation, the amorphous state boosts the photothermal effect.
Yang et al. [55]	Bi-RuO_2	The Bi-RuO_2 single-atom alloy oxide catalyst demonstrates a relatively low overpotential of 192 mV. It also shows excellent stability lasting over 650 h at a current density of 10 mA cm^{-2}. These properties make possible a practical PEMWE which requires merely 1.59 V to achieve a current density of 1.0 A cm^{-2} under industrial conditions.

3. Analytical Methods for NPCMs

In this section, we will concisely discuss the key methods pivotal for NPCM performance analysis. These mainly include Mechanism-oriented Analysis, which delves into fundamental interactions. Then there is Simulation-based Analysis, using computational models to accurately predict properties. Finally, Algorithm-driven optimization leverages algorithms to efficiently find optimal configurations for NPCM. Each method significantly contributes to a comprehensive understanding and enhances NPCM performance.

3.1. Mechanism-Oriented Analysis

Mechanism-Oriented Analysis is a crucial approach in understanding the behavior of NPCM in high-temperature thermal energy storage systems. This method delves deep into the fundamental mechanisms underlying the material's performance, aiming to establish a clear connection between its microscopic structure and macroscopic properties. At the microscopic level, NPCM consists of a base PCM embedded with NPs. These NPs can significantly alter the properties of PCMs. For example, they may enhance heat transfer by increasing the effective TC [56]. The mechanism-oriented analysis aims to explore how the size, shape, and distribution of these NPs interact with the molecular structure of the PCM, studying the interactions between NPs and the PCM which can affect the atomic morphology, pore structure, and chemical bond interactions within the PCM, thereby

influencing its heat storage and heat release capabilities [57,58]. By understanding these mechanisms, researchers can predict and optimize the performance of relevant NPCM. Commonly used mechanism-analysis methods for studying NPCM include molecular dynamics (MD) simulation, density functional theory (DFT), and stochastic simulation approaches, for which a review and analysis of the most recent relevant literature will be conducted hereinafter.

3.1.1. Molecular Dynamics (MD) Simulation

MD simulation has become an important tool for studying NPCMs with excellent performance. In research, MD enables researchers to delve deep into the complex atomic and molecular-level behaviors underlying the macroscopic properties of materials [59]. As shown in Figure 2, the corresponding atomic arrangement characteristics can be observed. For composite materials that are typically composed of matrix PCMs embedded with NPs, MD can accurately model the interactions between PCM molecules and NPs, which are of crucial importance as they significantly influence the thermal, mechanical, and phase change characteristics of the composite materials [60]. Additionally, MD assists in understanding the phase change processes in NPCM, which involve the complex phenomenon of PCMs transitioning from the solid to the liquid state or vice versa [61]. With the help of MD, researchers can track the energy changes, atomic displacements, and intermolecular forces during these phase transitions. The analysis of these principles is vital for optimizing the design of NPCM-based thermal energy storage systems, as it enables the optimization and regulation of phase change temperature, latent heat capacity, and other key parameters. In conclusion, MD plays a key role in uncovering the change mechanisms of NPCM and promoting the development of advanced thermal energy storage solutions. The following is an overview of the research on the application of the latest MD analysis method to the analysis of NPCM.

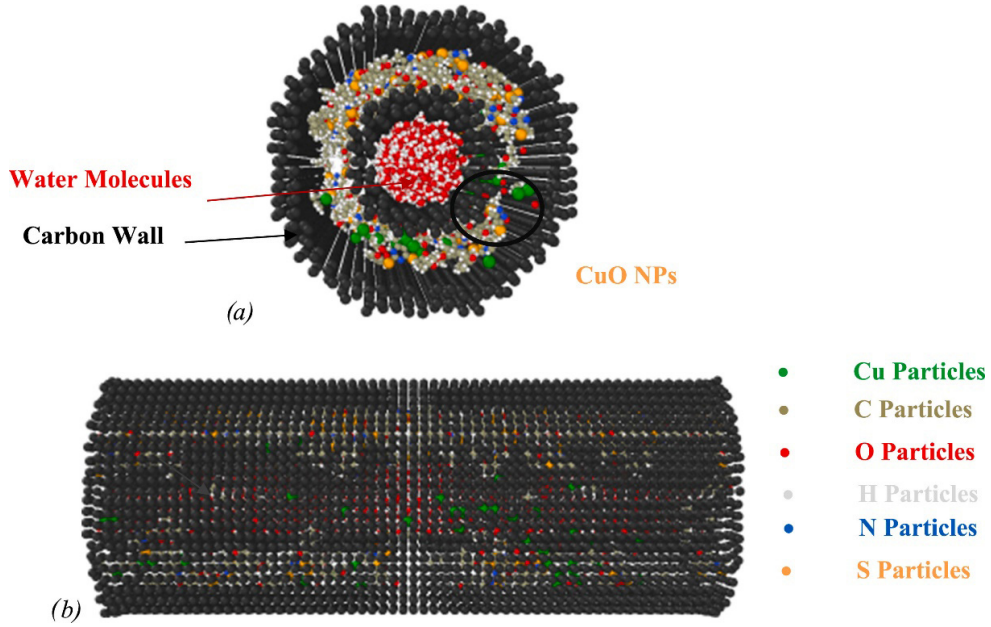

Figure 2. Schematic diagram of the atomic arrangement of SA-paraffin of CuO NPs. (Reproduced with permission from [60], Elsevier, 2025). (**a**) front view; (**b**) side view.

Cu NPs are frequently added to PCMs with the aim of enhancing the latter's thermal properties. Cu NPs are frequently added to PCMs due to their balanced cost, thermal conductivity, and chemical stability. Karimipour added Cu NPs to paraffin and analyzed the trends of TC and energy-efficiency transformation of paraffin-Cu-NFs placed between parallel plates under the influence of different panel temperatures [59]. Liu also used the

same materials in his study, where it was found that when the concentration of Cu NPs increased from 1% to 7%, the maximum density decreased by 1.62%, the maximum velocity increased to 0.00493 Å/fs, the maximum temperature increased by 3.9%, the heat transfer flux increased by 2.1%, the conductivity increased to 0.68 W/m·K, the charging time decreased by approximately 1.42%, and the discharging time decreased by approximately 0.14%, yet as the concentration of Cu NPs continued to increase to 10%, these parameters rebounded [62]. Singh's research also confirmed that different concentrations of Cu NPs had an impact on both TC and heat flux, but the turning-point concentration in the research results was 3%, which differed to some extent from previous studies, a difference caused by factors such as the setup of the simulation model and the force-field analysis method [63]. Cao carried out molecular-dynamics simulation and analysis using two types of PCM (hydrocarbon-water composite and paraffin) and three wall-metals (Pt, Cu, and Al), and found that the thermal performance of the combination of paraffin and Cu NPs was superior to that of other combinations [64]. Huang added Cu NPs to Sodium sulfate decahydrate and analyzed the heat and mass transfer process and phonon process [65].

CuO is also a high-quality NP. Gao analyzed the changing trends of the maximum velocity, temperature, TC, and heat flux of the SA/PCM/CuO nanostructure within a cylindrical pipe [66]. Yang considered the influence of the concentration of Cuo NPs on the thermal-performance parameters of the composite material, including density, maximum velocity, maximum temperature, heat flux, TC, charging time, and discharging time [67]. Ru discovered that when the atomic radius increased from 4 Å to 10 Å, the maximum density decreased to 0.0825 atoms/$Å^3$, the maximum velocity decreased, the maximum temperature dropped, TC decreased by 1.57 W/m·K, the charging time shortened by 6.09 ns, and the discharging time decreased by 8.28 ns [68]. An analysis was also conducted to evaluate the influence of the radius of NPs on these parameters. Notably, the charging time increased to 6.28 ns, which was contrary to the previous research results, so the study on the influence mechanism of the atomic radius on the charging time of the material still warrants further in-depth analysis [69]. Yu analyzed the influence of CuO NPs on the density, TC, and melting enthalpy of the lauric-acid PCM (as shown in Figure 3) [70]. Fang added SiO_2 NPs to the fundamental molten salt (a mixture of Na_2CO_3 and K_2CO_3) and analyzed the thermal conductivity and shear viscosity using MD [71]. The main materials and research contents of the above-mentioned study are listed in Table 3.

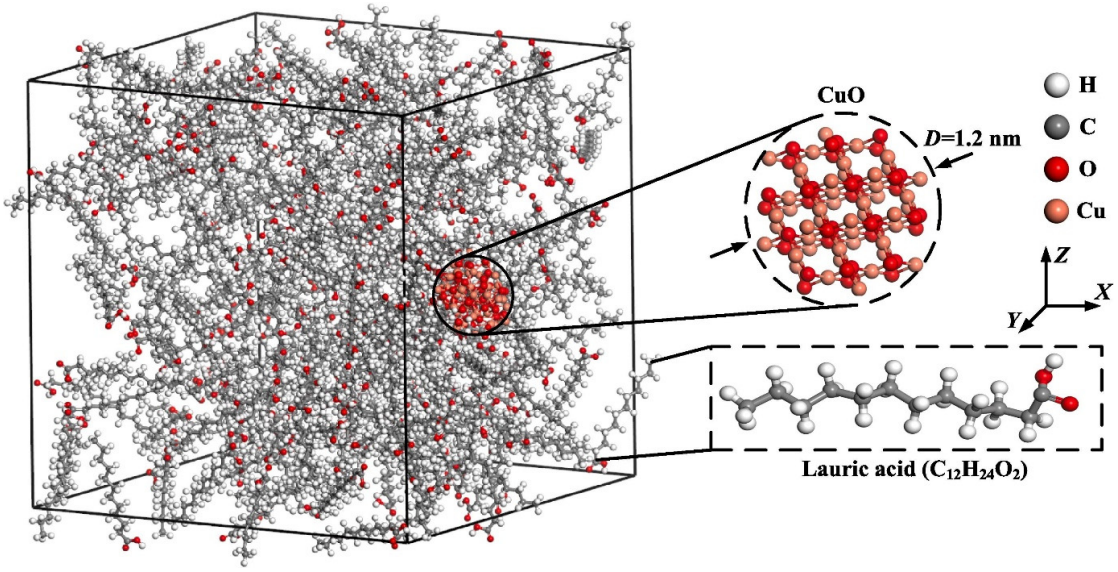

Figure 3. Schematic diagram of Lauric acid-CuO model (Reproduced with permission from [70], Elsevier, 2024).

Table 3. The main materials and research contents about MD.

Reference	Materials Set-Up	Analysis of Performance Improvement
Karimipour et al. [59]	Cu/paraffin	TC and energy-efficiency transformation
Liu et al. [62]	Cu/paraffin	7% Cu NPs: density, velocity, temperature, heat transfer flux, TC, charging time, discharging time
Singh et al. [63]	Cu/paraffin	3% Cu NPs: density, velocity, temperature, heat transfer flux, TC, charging time, discharging time
Cao et al. [64]	hydrocarbon-water composite, and paraffin/platinum, Cu, and Al)	The combination of paraffin and Cu NPs exhibits the highest cost-performance ratio in terms of thermal performance
Huang et al. [65]	Cu, Sodium sulfate decahydrate	TC, radius, diffusion coefficient, phonon density of states, phonon resonance, Debye temperature
Gao et al. [66]	Silica aerogel (SA)/PCM/CuO	velocity, temperature, TC, and heat transfer flux
Yang et al. [67]	SA/paraffin/CuO	The concentration of Cuo NPs: density, maximum velocity, maximum temperature, heat transfer flux, TC, charging time, and discharging time
Ru et al. [68]	SA/paraffin/CuO	The radius of Cuo NPs: density, velocity, temperature, TC, charging time, discharging time
An et al. [69]	SA/paraffin/CuO	The charging time increased to 6.28 ns
Yu et al. [70]	CuO/lauric-acid	density, TC, and melting enthalpy
Fang et al. [71]	a mixture of Na_2CO_3 and K_2CO_3, SiO_2	Thermal conductivity, shear viscosity, test factors, temperature

3.1.2. Density Functional Theory

In the research of NPCMs, DFT is an important quantum-mechanical method. At its core, it takes the electron density as the fundamental variable, positing that the ground-state energy of a system is a functional of the electron density [72]. Solving the relevant equations to determine the electron density significantly simplifies the computational complexity of multi-electron systems [73]. In the study of NPCM, DFT can precisely analyze the interactions between the base PCM and NPs at the atomic scale [74]. This helps in understanding how these interactions alter the heat transfer capabilities and other properties of NPCM. Moreover, DFT can delve deep into its phase change processes, facilitating the optimization of its applications in thermal energy storage and other aspects. Overall, DFT provides crucial support for unlocking the potential of NPCM in various applications.

As shown in Figure 4, Liang employed DFT to reveal enhanced van der Waals interactions and elevated non-covalent energy in acetylated lignin/fatty acid systems, achieving 40.8% particle yield, 57.2% fatty acid loading, and 70 °C phase transition temperature [75]. Zhang used DFT to demonstrate that graphitized carbon coating transforms non-uniform electric fields around Ni_0 NPs into spherical uniformity under solar irradiation [76]. Yao applied DFT to confirm 8.9 nm mesopore concentration in NPCM skeletons, aligning with scanning electron microscope (SEM) data [77]. Tan leveraged DFT-based quantum chemistry to prove modified lotus root starch enhances hydrogen bonding in sodium acetate trihydrate–sodium thiosulfate pentahydrate clusters, boosting water retention and thermal storage [78]. Yuan utilized DFT to characterize MIL-101(Fe) pore structures, identifying dominant 1.19 nm micropores and 15.17 nm mesopores [79]. Additional DFT studies include Wang's pore distribution analysis of a Zeolitic Imidazolate Framework-8 based biocompatible porous material of micron-size [80], Zeng's calculation of higher formation energy for C-substituted Sb_7Se_3 superlattices [81], and Xin's electronic density of states examination of Design and synthesize a composite PCM of $Na_2HPO_4{\cdot}12H_2O$ (DHPD)—vermiculite nanosheets (VMTNS) systems [82]. The main materials and research contents of the above-mentioned study are listed in Table 4.

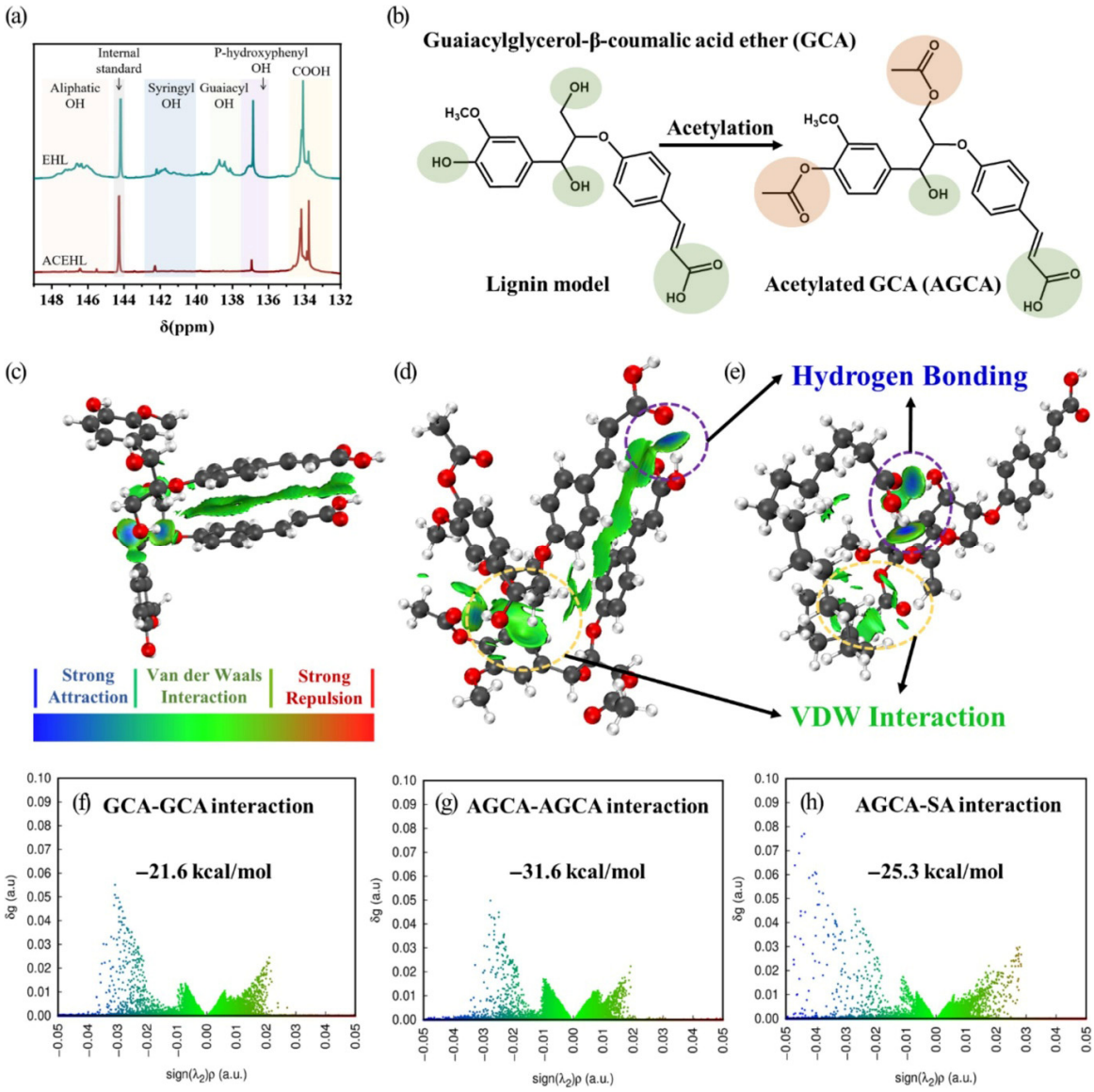

Figure 4. Analysis diagram of the formation mechanism of lignin-stearic acid capsules (Reproduced with permission from [75], Elsevier, 2025). (**a**) ^{31}P NMR spectra of EHL and ACEHL; (**b**) acetylation of GCA; (**c**–**e**) Isosurface and (**f**–**h**) scatter graph of independent gradient model based on Hirshfeld partitioning (IGMH) of the unacetylated lignin (GCA) dimer (**c**,**f**), acetylated lignin (AGCA) dimer (**d**,**g**), AGCA combined with stearic acid (**e**,**h**).

Table 4. The main materials and research contents about DFT.

References	Materials Set-Up/References	Research Methods	Research Points
Liang et al. [75]	Lignin fatty-acid capsules were prepared using an anti-solvent method after lignin was modified with a 6:4 ethanol-ethyl acetate mixture.	Characterization: Transmission electron microscope (TEM), Dynamic light scattering, Fourier transform infrared spectroscopy (FTIR), Nuclear magnetic resonance, X–ray photoelectron spectroscopy (XPS), Differential scanning calorimetry (DSC), Thermogravimetric analysis (TGA), DFT. Model: MD, Independent gradient model based on Hirshfeld Partitioning.	The solubility matching problem between lignin and stearic acid. The interaction relationship between lignin and stearic acid. A self-assembly mechanism for acetylated lignin and stearic acid. The heat storage performance, supercooling degree, and thermal stability of the modified lignin-stearic acid nanocapsules

Table 4. *Cont.*

References	Materials Set-Up/References	Research Methods	Research Points
Zhang et al. [76]	Octadecanol (ODA) is encapsulated into the hierarchically porous carbon structure infiltrated with Ni@graphite (Ni@C/C).	Characterization: SEM, nitrogen adsorption-desorption isotherm, TEM, Energy-Dispersive Spectroscop, X–ray diffraction, raman spectroscopy XPS, FTIR, TGA, DSC, UV-Vis-NIR spectroscopy, DFT. Models: Analytical method for phase change kinetics, MD, Zhishen Mo method, mean square displacement.	The crystallization characteristics of the PCM and Ni@C/C. The interaction energy, radius of gyration, kinetic energy, and diffusion coefficient between the PCM and Ni@C/C. The crystallization time and relative crystallinity of the pristine ODA and ODA/Ni@C/C. The non-isothermal charging and discharging performance, Localized Surface Plasmon Resonance effect, photothermal conversion ability, heat release characteristics, and extreme cold-heat management capacity of ODA/Ni@C/C-4.
Yao et al. [77]	The radio-frequency polymer framework (in-situ polymerized in the presence of a sodium hydroxide catalyst) and the phase change component (resorcinol (R) and furfural (F) are dissolved in molten phase change component).	Characterization: FTIR, SEM, Nitrogen adsorption-desorption isotherm, Brunauer–Emmett–Teller (BET), DSC, TC Test, Heat conductivity coefficient test, Leakage rate analysis, DFT, Flexural strength test, Temperature control test.	The adsorption effect between the RF framework and phase change component. Analyzed the mesoporous nanostructure characteristics of RF-PF. The mass retention rate, shape stability, TC, and contact thermal resistance of the RF- composite PCM specimens. The temperature and temperature difference of the RF- composite PCM plates
Tan et al. [78]	The composite PCM is prepared by using high-density carbon-nanofiber encapsulation of modified broad-leaved root starch enhanced with carbon nanofibers and graphene nanosheets and choosing sodium acetate trihydrate and sodium thiosulfate pentahydrate.	Characterization: DSC, SEM, X–ray diffractometer (XRD), TC analysis, Viscosity analysis, DFT.	The pore structure characteristics, interactions, solidification characteristics, crystallization characteristics, TC, melting enthalpy, and molecular structure features of the composite material.
Yuan et al. [79]	Tetradecanol is confined in the micro-mesopores of the MIL-101(Fe) nanoporous supporting matrix.	Characterization: BET, DFT, Porosity analysis, SEM, XRD, FTIR, DSC, TGA, Thermal cycling stability, Phase change loading rate test.	The interaction between MIL-101(Fe) and tetradecanol. The pore characteristics, adsorption characteristics, and crystallization characteristics of the composite PCM. The influence of different concentrations of tetradecanol on the phase change enthalpy transformation process of the composite material, weight loss rate and weight loss temperature, cycle stability, melting process characteristics, hydrothermal tolerance, and material loss degree.
Wang et al. [80]	Porous Zeolitic Imidazolate Framework-8 Microcrystal/Doxorubicin Hydrochloride @ Tetraol-Polydopamine Composite Material	Characterization: FTIR, TEM, XRD, SEM, Thermal infrared imaging, BET, DFT, Dynamic light scattering, Zeta potential analysis, Nanodrop one spectrophotometer	Drug release behaviors at different pH values and temperatures. The morphological characteristics, pore size characteristics, drug-loading capacity, and photothermal conversion ability of the composite material.
Zeng et al. [81]	Prepare C/Sb_7Se_3 thin film using Sb_7Se_3 and C materials.	Characterization: Magnetron sputtering instrument, XRD, Raman spectroscopy, near-infrared spectrophotometer, XPS, X–ray reflectometry, Atomic force microscope, Ion thinning process, Dual-beam focused ion beam process, TEM, Model: Utilize a signal system constructed from an arbitrary waveform generator, a digital source meter, and a micro-control probe observatory. Employ the Vienna ab initio simulation package, the projector-augmented wave potential, the generalized gradient approximation of Perdew–Burke–Ernzerhof, and DFT-D2.	Amorphous resistance characteristics, crystalline resistance characteristics, crystallization activation energy, crystallization process, grain size, interactions, and wide bandgap of the thin film

Table 4. *Cont.*

References	Materials Set-Up/References	Research Methods	Research Points
Xin et al. [82]	DHPD-VMTNS with both surface and confined space using $Na_2HPO_4 \cdot 12H_2O$.	Characterization: X–ray fluorescence, field emission scanning electron microscope, TEM, Atomic force microscopy, Zeta potential, XRD, FTIR, DSC, Constant-temperature water-bath method, TGA, DFT. Model: MD, optimization method of CASTEP software package, universal force field, analysis of electrostatic force and van der Waals force, Gamma analysis based on ultrasoft pseudopotential.	The interaction and diffusion mechanism between VMT and DHPD. The adsorption characteristics, crystallinity, compatibility, morphological features, phase change and heat storage properties of DHPD in VMTNS.

3.1.3. Characterization Method

Characterization methods, which involve using experimental equipment to collect relevant signals and conduct principled analyses of specific material properties, are employed to better observe the microstructure and performance characteristics of NPCMs when applied to their analysis. This provides crucial support for developing new high—heat and high—stability NPCMs. Multiple experimental approaches are often combined with modeling techniques for analyzing a single NPCM material. Common characterization techniques include SEM, TEM, XRD, FTIR, DSC, TGA, and Temperature history methods (T-history methods). SEM is commonly employed to observe the microstructure and offers a high-resolution surface view [83,84]. TEM is also utilized for microstructure observation, but it enables internal-structure analysis at the micro-scale [85,86]. XRD is utilized to determine the crystal structure of NPCM components [87,88]. FTIR identifies functional groups by detecting chemical bond vibrations [89,90]. DSC was employed to characterize its unique thermal properties, including thermal hysteresis, phase transition temperature, latent heat, and thermal stability [91,92]. TGA is employed to investigate its phase change characteristics [93,94]. The T-history method is used to analyze the temperature curves of NPCM and further derive the thermophysical properties of the materials [95,96]. The main materials and research contents of the above-mentioned study are listed in Table 5.

Table 5. The main materials and research contents about characterization methods.

Research Method	Research Content	Ref.
SEM	Observe the surface morphology and microstructure of NPCM and assess its particle size and distribution.	[83,84]
TEM	Analyze the internal microstructure of NPCM and examine its crystalline structure and defects.	[85,86]
XRD	Identify the crystalline composition and crystallinity of NPCM and investigate its phase transition.	[87,88]
FTIR	Detect functional groups and chemical bonds in NPCM and investigate its chemical structure and interactions.	[89,90]
DSC	Analyze the thermal properties of NPCM, including thermal hysteresis, phase transition temperature, latent heat, and thermal stability.	[91,92]
TGA	Assess the thermal stability and decomposition temperature of NPCM and investigate its thermal decomposition process and composition.	[93,94]
T-history methods	Analyze the temperature curves of NPCM and research the thermophysical properties of the materials.	[95,96]

3.2. Simulation-Based Analysis

Simulation-based analysis plays a pivotal role in the study of NPCM within high-temperature thermal energy storage systems. This approach utilizes computational models to replicate and analyze the complex behaviors of NPCM, offering insights that are often difficult to obtain through experimental means alone. In Simulation-Based Analysis, various physical phenomena such as heat transfer, phase transitions [97], and fluid flow within the NPCM are numerically modeled. For heat transfer, models consider the enhanced TC imparted by the NPs in NPCM. They simulate how heat diffuses through the composite material, taking into account the interactions between the base PCM and the NPs. When it comes to phase transitions, simulations can precisely capture the temperature-dependent behavior of NPCM. By inputting the thermo-physical properties of the components, these models can predict the onset and duration of phase changes, which are crucial for understanding the energy storage and release processes. Moreover, in systems where NPCM might be used in flowing configurations, fluid-flow simulations help analyze how the presence of NPs affects the flow characteristics. This information is valuable for designing efficient heat exchange systems. Overall, Simulation-Based Analysis provides a cost-effective and time-efficient way to explore different scenarios, optimize NPCM-based systems, and guide experimental research. Commonly used simulation-based analyses for studying NPCM include finite element analysis (FEA), computational fluid dynamics (CFD), stochastic simulation approaches, and multiphysics coupling models, for which a review and analysis of the most recent relevant literature will be conducted hereinafter.

3.2.1. Finite Element Analysis

FEA discretizes complex structures into finite elements to build simulation models, predicting the temperature field, stress distribution, and energy transfer efficiency of materials during phase transitions [98,99]. FEA can quantitatively analyze the impact of NP dispersibility on the thermal performance parameters of PCMs, thereby optimizing the design of porous encapsulation to reduce the leakage rate. Meanwhile, it simulates the regulatory mechanism of nanoscale interfacial thermal resistance on phase—change kinetics at the micro—scale, providing theoretical support for the efficient thermal management of NPCMs in scenarios such as electronic heat dissipation and intelligent buildings. The following is an overview of the research on the application of the latest FEA analysis method to the analysis of NPCM.

Gürsoy investigated the thermal performance of RT58-based composites incorporating spherical, square, and elliptical dimpled fins with varied Al_2O_3 NP concentrations [100]. Hekmat explored heat transfer enhancement in a spiral circular thermal storage system (as shown in Figure 5) using RT-50 with differently dosed NPs [101]. Dora developed a hierarchical composite by blending nano-silica/coconut fiber with decanol-ethanol-treated exfoliated vermiculite PCM, subsequently integrating it into foam concrete for building thermal analysis [102]. Yang engineered graded-porosity foam Cu/paraffin NPCMs to optimize structural configurations based on porosity uniformity, thermal response, and energy storage dynamics [103]. Lastly, Zhao quantified Herringbone Graphite Nanofiber agglomeration effects in paraffin via spherical clustering and linear percolation models, revealing enhanced TC in linear networks under high interfacial conditions [104]. Sun used artificially cultivated diatom microcrystals to modulate carbilose nanofibers to fabricate porous frameworks to fabricate PCMs with stable shapes, and modeled and studied the influence of pore properties on leakage resistance (as shown in Figure 6) [105]. Çiçek established a symmetric radiator model to analyze the effects of different NP concentrations and heat flux on thermal performance [56]. Saleh modeled the flexible structure of a square cavity using the Arbitrary Lagrangian–Eulerian method and analyzed the effects of

temperature, Stefan number, and other factors on the system's overall performance [106]. Egami added CuO nano-powders to PCM in a rectangular container with H-shaped fins, analyzing the effects of nano-powders' concentration and shape factor on freezing performance [107]. The main materials and research contents of the above-mentioned study are listed in Table 6.

Table 6. The main materials and research contents about FEA approaches.

Reference	Materials Set-Up	Simulation	Analysis Method	Key Parameters
Gürsoy et al. [100]	RT58 paraffin, Al-based metal foam, nanoscale particles of Al_2O_3	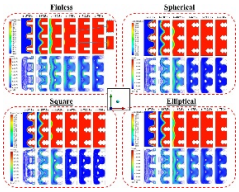	Spherical, square and oval rectangular containers with integrated structural walls; Based on the finite volume method, the Brinkman–Forchheimer extended Darcy model and the local thermal equilibrium model, the enthalpy-porosity method.	Melting time, temperature difference, Nusselt (Nu), energy change, energy storage parameters.
Hekmat et al. [101]	RT-50, Al_2O_3 NPs	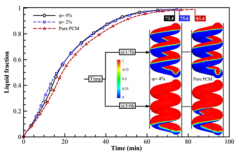	Three-dimensional spiral circular structure; Enthalpy-porosity model and Boussinesq approximate.	Melting time, solidification time, volume fraction NPs, feed port temperature, Reynolds number.
Dora et al. [102]	Nano silica/coir, decanol-ethanol treated stripped vermiculite, concrete	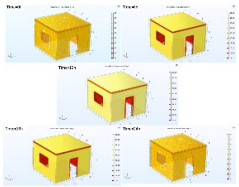	3D heat transfer building model; A general heat conduction equation for structures with no internal heat source.	TC, compressive strength, melting and freezing parameters, latent heat capacity, mass loss, compatibility and high heat resistance.
Yang et al. [103]	Cu foam/paraffin	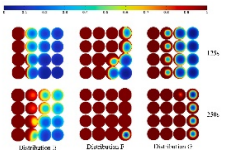	Tetrahedral models of elements with different porosities, continuity equations, energy equations, heat transfer mechanisms.	Porosity uniformity, temperature difference, heat storage capacity.
Zhao et al. [104]	Cu foam, carbon fiber reinforced plastic composite and octadecane	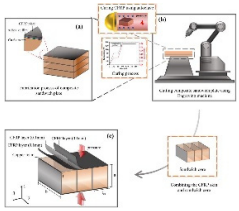	A multifunctional thermal management composite sandwich structure: 3D failure model, universal testing machine, 2D transient numerical model.	Specific strength, specific energy, composite plate thickness, thermal rate, TC.
Sun et al. [105]	Artificially cultured diatom microlenses regulate carbocellulose nanofibers	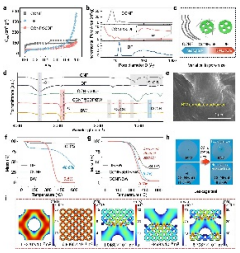	Multi-level pore model, SEM, XPS, Al Kα radiation, Raman spectroscopy, N2 adsorption and desorption isotherms, BET, Barrett–Joyner–Halenda, FTIR, TGA	Shrinkage, specific surface area, enthalpy of phase-change, TC.

Table 6. *Cont.*

Reference	Materials Set-Up	Simulation	Analysis Method	Key Parameters
Çiçek et al. [56]	Fe_3O_4, MgO, ZnO, and xGNP, added to RT-35HC with volume fractions of 0.02, 0.04, and 0.06. Al6061 as a heat sink and fin material	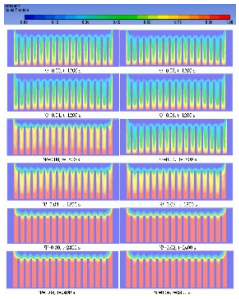	A symmetrical 3D NPCM heat sink (114 × 114 × 25 mm) model was constructed using Ansys fluent to analyze the effect of the input heat flux generated by the heater cap (100 × 100 × 1 mm) with a grid and a duration of 900,000 and 1 s. Continuity momentum equation, energy equation, thermal conductivity equation, viscosity equation.	NP type, vessel temperature profile, melt profile, melting time and volume fraction, reference temperature, thermal conductivity, heat flux.
Saleh et al. [106]	Nano-capsules are structured with polyurethane as the outer shell and nonadecane as the inner core.	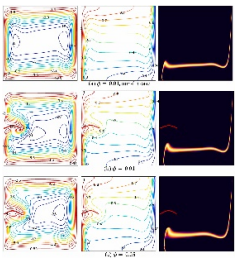	The square cavity filled with nano—encapsulated PCM and a base fluid has a fin of variable length at the midpoint of its left side. The Arbitrary Lagrangian–Eulerian method, Boussinesq approximation, Laplace equation, and Winslow formula.	Rayleigh number, Stefan number, fusion temperature, Capsule PCM concentration, Melting temperature, Young's modulus.
Egami et al. [107]	CuO nano-powders, PCM	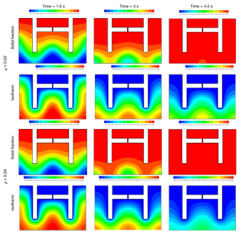	A rectangular container with H-shaped fins. Galerkin Method.	Concentration and shape factor of nano-powders

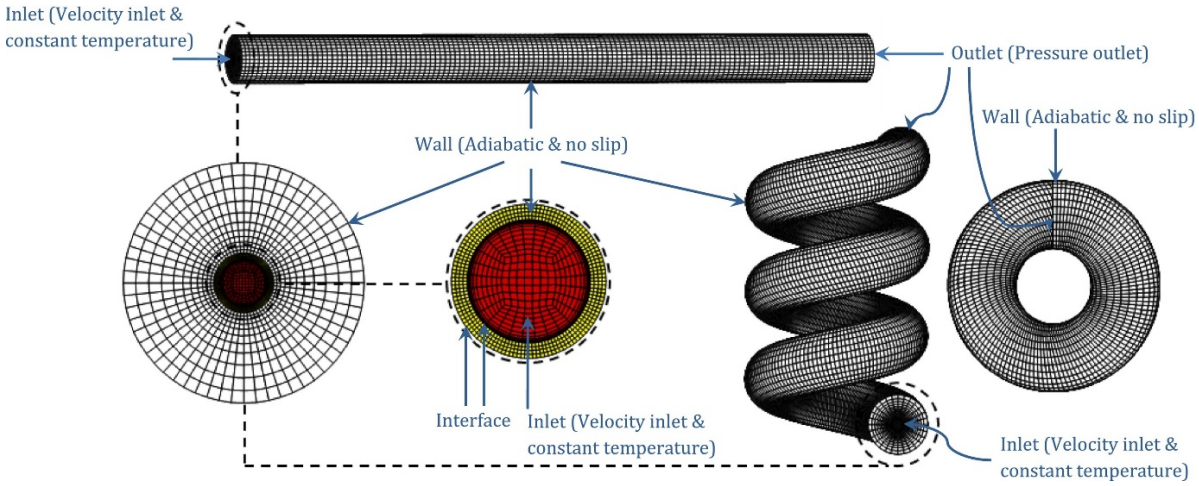

Figure 5. Schematic diagram of the three-dimensional spiral circular structure (Reproduced with permission from [101], Elsevier, 2025).

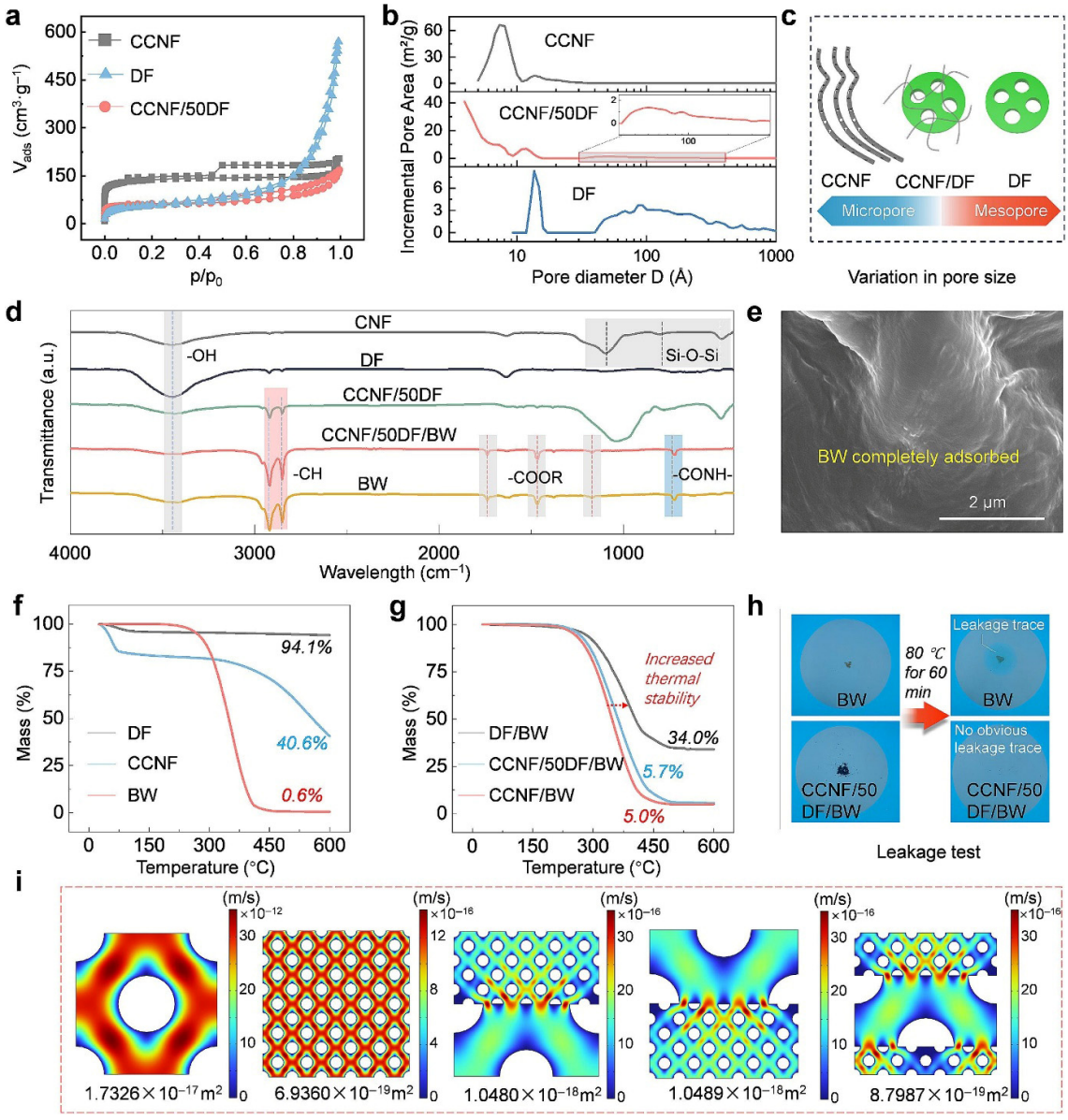

Figure 6. Simulation analysis of carbilose nanofibers and the impact on leaks (Reproduced with permission from [105], Elsevier, 2025). (**a**) N_2 isothermal adsorption–desorption curves; (**b**) pore size distribution of CCNF, DF, and CCNF/50DF; (**c**) pore size regulation; (**d**) FTIR spectra of the CCNF composite porous framework and BW composites; (**e**) SEM image of CCNF/50DF/BW. TGA curves of (**f**) CCNF, BW and DF as well as (**g**) the prepared ss-PCMs. (**h**) Schematic diagram of liquid flow in the porous framework, along with (**i**) simplified 2D models constructed.

3.2.2. Computational Fluid Dynamics

CFD plays a key role in the study of NPCM applications as a powerful tool for simulating fluid flow and heat transfer phenomena [108,109]. NPCMs use the phase transformation process to absorb or release a large amount of latent heat, but their thermal properties are highly dependent on the nanoscale structure of the material itself, its dispersion stability, and its interaction with the surrounding fluid. By simulating complex multiphase flow systems containing NPCM particles or capsules, CFD can reveal micro/macroscale flow, heat transfer, and phase transition coupling mechanisms to guide the design of NPCMs and evaluate their thermal management performance in energy storage systems. The following is an overview of the research on the application of the latest CFD analysis method to the analysis of NPCM.

Olivares-Robles designed a ring thermoelectric cooler composed of semiconductors, PCM (OM32 and Polyethylene glycol 1500), base fluid (water), and Al_2O_3 NPs, and analyzed the effects of NP concentration and temperature on the thermal performance of the cooler [110]. Benyahia developed a simulation model of a finned triangular inner tube and paraffin PCM enhanced with Cu NPs to analyze the effects of different NP concentrations, tube eccentricity, and inclination on the thermal properties of materials [111]. Bouzennada established a simulation model of NPCM fluids contained in different wave side wall cavities to analyze the influence mechanism of different wall structures, cylindrical radii, and rotational speed (as shown in Figure 7), and NPs concentration on thermal performance [112]. Glolami built Cu fins and Al heat sinks, analyzed the phase transformation process of $Na_2SO_4 \cdot 10H_2O$, paraffin, and eicosane, and analyzed the efficiency of photovoltaic panels [113]. Nandi used CuO NPs, lauric acid, RT35HC, and P58 materials to analyze the affected mechanism of improved solar irradiation by designing a rectangular geometry with different parallel structure shapes [114]. Shaik used CuO NPs, RT82, to analyze the effects of different liquid fractions and shapes on melting time and melting rate by designing a modified fin (as shown in Figure 8) with different vertical structure shapes [115]. Waqas used multi-walled carbon nanotube (MWCNT), TiO_2, and molten-salt PCM materials to design different rotationally symmetrical fin structures in hollow cylinders (as shown in Figure 9) to analyze the thermal performance of tubular heat exchangers [116]. Mahdavi designed PV laminates using Cu NPs, porous Cu media, and RT35-HC paraffin, and analyzed the effects of water pipe placement, NP concentration, and porous media on the thermal and electrical energy of the PV panels [117]. Alam analyzed the melting performance of latent heat thermal energy storage units made of different materials and shaped PCM [118]. Kiyak analyzed the effect mechanism of curvature and different concentrations of Cu NPs on the melting and solidification processes of thermal energy storage systems [119]. The main materials and research contents of the above-mentioned study are listed in Table 7.

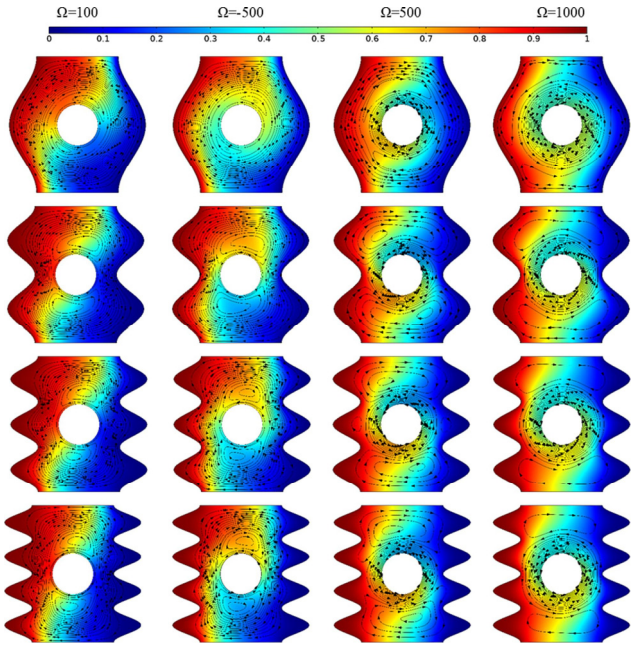

Figure 7. Simulation results under different wall structures and speeds (Reproduced with permission from [112], Elsevier, 2024).

Table 7. The main materials and research contents about CFD approaches.

Reference	Materials Set-Up	Simulation	Analysis Method	Key Parameters
Olivares-Robles et al. [110]	OM32 and Polyethylene glycol 1500, Al_2O_3 NPs	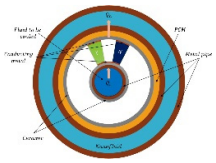	The annular thermoelectric cooler model consists of p-type and n-type semiconductor components made of bismuth telluride (Bi_2Te_3), with the components insulated by a ceramic plate and cooled using PCM. Finite difference method discrete transient equations	Coefficient of performance, TC, Reynolds number, Prandtl number, Nu, NP concentration
Benyahia et al. [111]	Paraffin, Cu NP	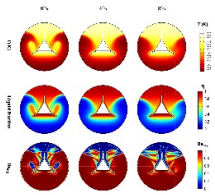	The cylindrical shell of the inner hollow triangular tube was established; the two-dimensional axisymmetric formula was used to simulate the thermal and flow behavior in the latent heat thermal energy storage (LHTES) element, the numerical solution was obtained by the generalized α time integral method, the second-order Lagrangian finite element was spatially discretized with a time step of 1 s, Boussinesq approximate, the Carman–Kozeny relation kinetic energy equation, and the Carman–Kozeny equation	The concentration of Cu NPs, TC, melting time, inclination angles, Nu, eccentricity, porosity
Bouzennada et al. [112]	Polyurethane/Nonadecane dispersed in water	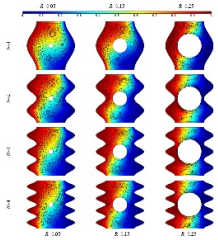	A 2D enclosed body filled with NPCM fluid; Galerkin weighted residual finite element method, Galkin weighted residual finite element method	Volume fraction, cylindrical radius, rotational speed, melting temperature, flow structure, heat transfer rate, Stefan number, Nu
Gholami et al. [113]	$Na_2SO_4{\cdot}10H_2O$ was mixed with Al_2O_3 and MgO NPs, paraffin and eicosane	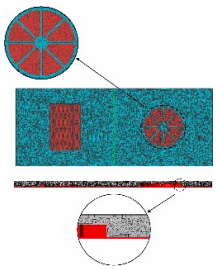	A photovoltaic panel and PCM cavity structure were established; A first-order upwind approach for the discretization of the momentum equation and a second-order approach for the energy equation, and a second-order scheme for the energy equation	the concentration of NPs, efficiency and temperature
Nandi et al. [114]	CuO NPs, lauric acid, RT-35HC and P-58	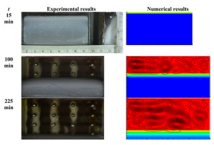	a rectangular geometry characterized by specific dimensions	The concentration of NPs, fin structure, energy storage rate, melting rate
Shaik et al. [115]	CuO NPs, RT82	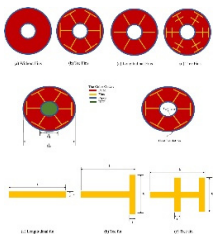	PISO method, PRESTO, second-order upwind methods, second-order upwind algorithms	NP concentration, shape, melting time, melting speed

Table 7. *Cont.*

Reference	Materials Set-Up	Simulation	Analysis Method	Key Parameters
Waqas et al. [116]	MWCNT, TiO_2, molten-salt PCM	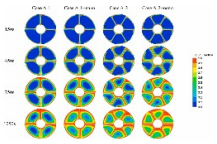	Boussinesq approximation, Semi-implicit method for pressure linked equations (SIMPLE), PRESTO system	Fin shape, compactness, melting time
Mahdavi et al. [117]	Cu NPs, porous Cu media, and RT35-HC paraffin	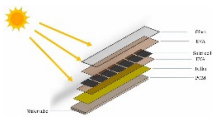	Five-layer PV panels; discrete ordinate method; Boussinesq approximation	Electrical efficiency, economic analysis, pipe placement, NP concentration
Alam et al. [118]	n-Octadecane, Capric acid, MWCNTs, Cu metal foam	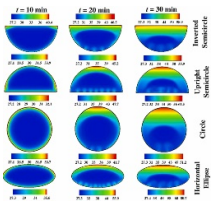	A two-dimensional computational model of square geometry, finite volume method	Enclosure geometries, Prandtl numbers, Grashof number, Stefan number, NPs concentration, melting rate
Kiyak et al. [119]	CuO NPs, RT19HC	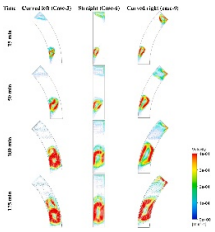	a curved geometry and a straight geometry; the Navier–Stokes equations, enthalpy-porosity technique. Boussinesq approximation, finite volume method, SIMPLE, the implicit Euler method	Nu, concentration of NPs, geometric curvature, phase change time, melting time, discharge efficiency

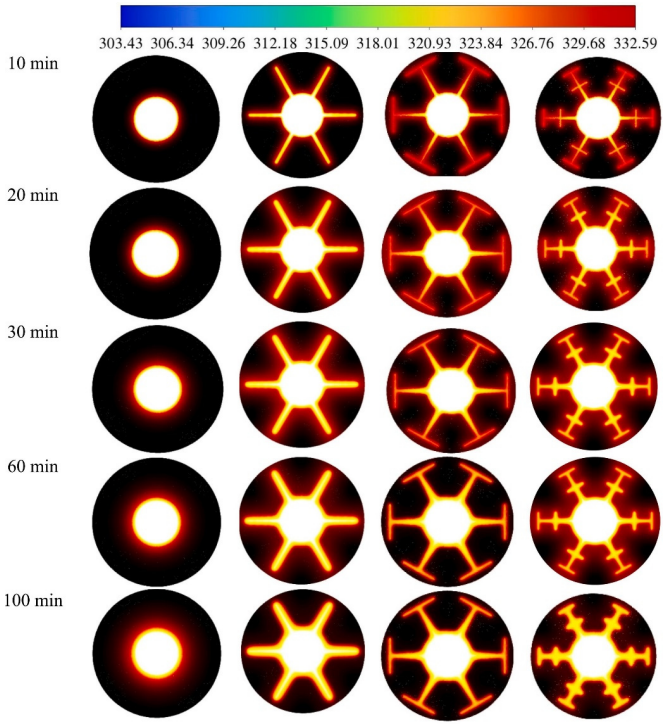

Figure 8. Simulation results of modified fin with different parallel structure shapes (Reproduced with permission from [115], Elsevier, 2025).

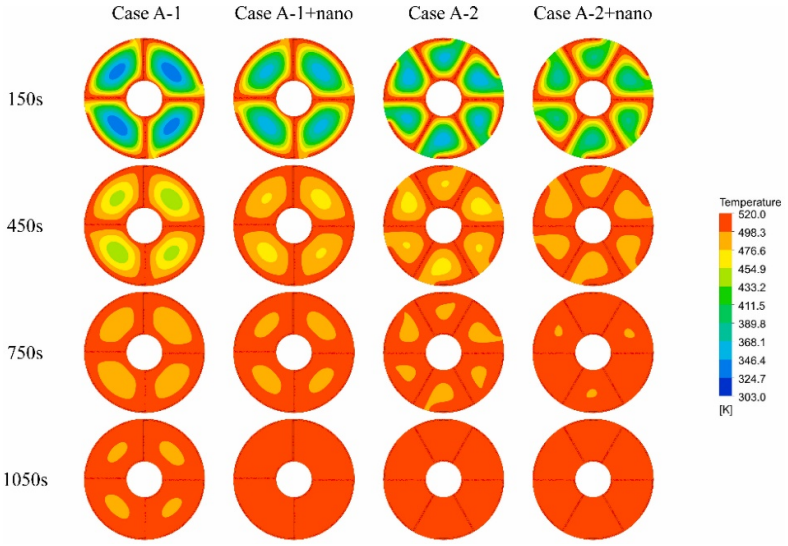

Figure 9. Simulation results of different rotationally symmetrical fin structures (Reproduced with permission from [116], Elsevier, 2025).

3.2.3. System Performance Simulation

System performance simulation provides core support for design optimization by building a highly integrated system simulation coupling model to efficiently simulate the overall dynamic response and comprehensive performance of complex systems in an experimental or simulation environment. With its high thermal conductivity, latent heat of phase change, and fast response, NPCMs are often used in the design of various photothermal conversion system materials, which enhance the performance characteristics of the system in thermal management or electrical efficiency management, accelerate the research and development of photothermal systems, and improve the reliability of the system. The following is an overview of the research on the application of the latest system performance simulation analysis method to the analysis of NPCM.

Amin added graphene to beeswax to make distillation tubes and designed an experimental system for analyzing freshwater production performance by combining K-type thermocouples, insolation intensity meters, graduated cylinders, and data collectors [120]. Singh added different concentrations of Al_2O_3 particles to OM37 to make NPCMs for the analysis of the thermal performance of solar ponds [121]. Emara integrated the design of a freshwater system by adding different concentrations of TiO_2 and Al_2O_3 nanofluids to paraffin with a melting temperature of 62 °C [122]. Al-Karboly integrated a twisted band absorber, a twisted absorption tube, a 1% SiC NP-reinforced paraffin preparation vessel, and a silicon carbide nanofluid, comprehensively designed a photovoltaic system (Shown in Figure 10), and analyzed its thermal efficiency [123]. Kamrava used ZnO, CuO, and Al_2O_3 in paraffin wax as NPCM to further construct the floor heating system and analyzed the thermal performance characteristics of the floor temperature and heat flux of the floor heating system [124]. Gür added B_4C to the RT35HC to design the heat sink, further constructed an ultra-low energy consumption home heat sink simulation system, and analyzed the thermal performance factors such as room temperature and water temperature [125]. Sathishkumar used GNP and strong nitric acid to prepare NPCM materials to design the energy storage tank system, and analyzed the thermal performance parameters such as stored energy and solidification time [126]. Bassam used nanofluids (SiC and water preparation) and NPCM (SiC and paraffin preparation) to design micro-finned tubes, and the comprehensive design of the photovoltaic system showed a 77.5% increase in thermal efficiency and an increase in output power to 14.5 W [127,128]. Kibria used NPCM (paraffin

wax with Al_2O_3 and ZnO NPs) to design a photovoltaic thermal system, and the analysis results showed that the surface temperature of the system was reduced by 5.4 °C, the power was increased by 2.75%, the electrical efficiency was increased by 2.71%, the maximum heat output power was increased by 17.4%, and the overall efficiency was increased by 15.82% [129]. Bharathiraja designed a collector system incorporating MWCNTs and SiO and discovered that this design led to a higher output temperature and a longer duration for hot water production [130]. The main materials and research contents of the above-mentioned study are listed in Table 8.

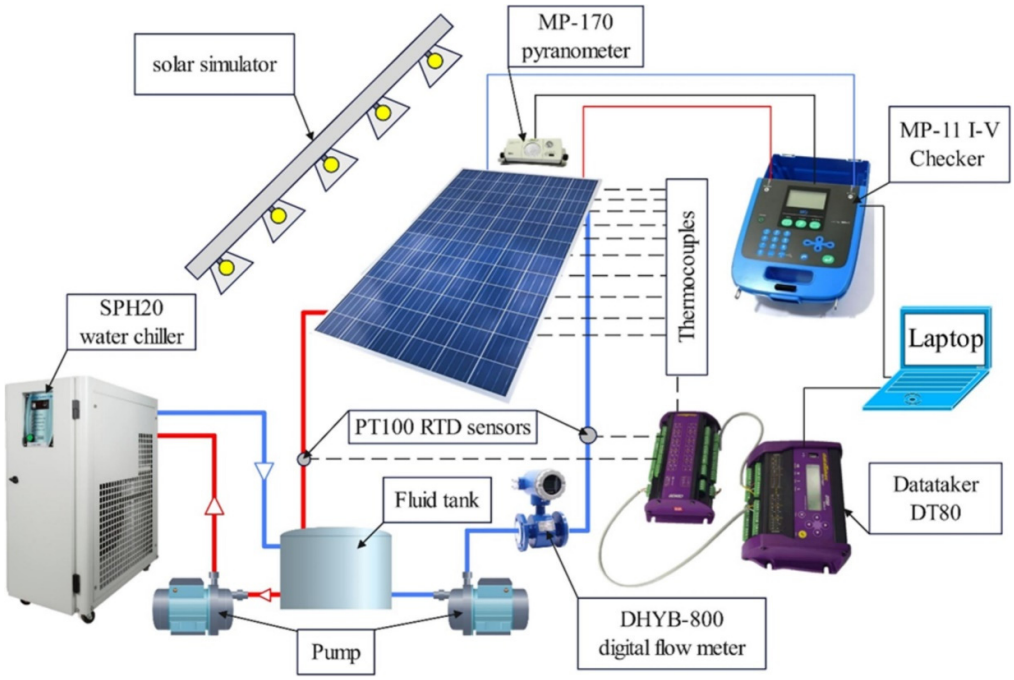

Figure 10. Photovoltaic system (Reproduced with permission from [123], Elsevier, 2025).

Table 8. The main materials and research contents about system performance simulation approaches.

Reference	Materials	System	Devices	Key Parameters
Amin et al. [120]	Graphene, beeswax	Freshwater production	Distillation tubes, K type thermocouples, insolation intensity meters, graduated cylinder connections, data acquisition equipment	Ambient temperature, solar radiation, thermal conductivity, temperature, freshwater productivity, thermal efficiency, energy efficiency
Singh et al. [121]	Al_2O_3, OM37	Solar ponds	Data collectors, thermocouples, solar pond installations	Latent calorific value, thermal conductivity, thermal power, thermal efficiency
Emara et al. [122]	TiO_2, Al_2O_3, paraffin	Distilled water	Radiators, water tanks and their heaters, liquid supply tanks, centrifugal pumps, fans, flow meters, thermocouples, temperature sensors, temperature indicators, solid state relays	Flow rate, rotational speed, heat transfer coefficient, NP concentration
Al-Karboly et al. [123]	SiC, PCM	PV	Solar simulator, pyranometer, I-V checker, Laptop, datataker, digital flow meter, pump, fluid tank, water chiller, RTD sensors, Themocouples	Electrical efficiency, thermal efficiency, overall efficiency, nanofluid concentration
Kamrava et al. [124]	ZnO, CuO, Al_2O_3, paraffin	Underfloor heating	A structured framework for integrating NPCMs	NP concentration, floor temperature, heat flux, thermal conductivity, melting time
Gür et al. [125]	B4C, RT35HC	radiator	PVT collectors, heat sinks, PCM layers, Cu tubes	Water temperature, room temperature, heat retention

Table 8. *Cont.*

Reference	Materials	System	Devices	Key Parameters
Sathishkumar et al. [126]	GNP, strong nitric acid	energy storage tank	A chiller unit, energy storage tank, circulating pump, flow meter and energy meter	Flow rate, desolidification time, charging time, melting time, heat transfer rate, temperature, charging power, voltage drop, latent heat energy, accumulated energy, specific energy consumption
Bassam et al. [127,128]	SiC, paraffin, Polyvinylpyrrolidone	PV	Fluid tank, pump, flow meter, data logger, photovoltaic panel, pyranometer, I–V curve checker, computer cooling unit, heat exchanger, PCM expansion tank	Electrical efficiency, thermal efficiency, temperature
Kibria et al. [129]	Al_2O_3, ZnO, paraffin,	PV	PV, hot water storage, PVT/PCM, Structure, PVT/HNPCM, water tap, overhead tank, pipes	Thermal conductivity, latent heat capacity, temperature, electricity efficiency
Bharathiraja et al. [130]	MWCNTs, SiO	Collector	Cup type anemometer, data logger, solar intensity meter, laptop, storage tank, copper tube embedded PCM, thermocouple, absorber plate	Outlet water temperature, temperature, hot water time

3.2.4. Magnetic Field Coupling Models

The magnetic field changes the Lorentz and Kelvin forces in the convective heat transfer process through the coupling of the changes in magnetic induction intensity with the conductivity and magnetism of different NPs. This regulates the melting and solidification behaviors in the phase transformation process of the NPCM, further altering the relevant thermodynamic characteristic parameters of the NPCM. Additionally, the coupling effect can also impact the dynamic behavior between NPs and PCM, resulting in current changes that adjust the system's charging and discharging processes, thereby optimizing the system's power characteristic parameters [131]. The following is an overview of the research on the application of the latest magnetic field coupling models analysis method to the analysis of NPCM.

Izadi added different concentrations of Al_2O_3 nanoadditives to paraffin wax to construct a hexagonal heat storage unit and analyzed the convective melting mechanism of the tilt angle and magnetic field strength [132]. Hassan designed a U-shaped baffle cavity for the nano-encapsulated PCMs and analyzed the mechanism of the natural convection effect of the inclined magnetic field on the structure [133]. Younis designed a cavity structure to analyze the mechanism by which magnetic field strength affects the thermal properties of nano-encapsulated PCMs [134]. Selimefendigil designed a triangular-shaped structure containing Ag-MgO hybrid nanofluids to analyze the convective influence mechanism in a heterogeneous magnetic field [135]; designed a multi-jet impingement system to study the numerical effects of Ag-MgO nanofluids on the thermal properties of PCMs under different magnetic field strengths and clarity [136]; studied the phase transition and convective heat transfer mechanisms of different types of NPs and encapsulated PCMs under magnetic fields [137]. Nguyen designed an external magnetic field for the analysis of the thermal performance effects of NPCM capsules incorporated into roof structures [138]. Lu designed a stable rotating magnetic field applied to paraffin wax doped with Fe_3O_4 to analyze the effect of the magnetic field on the melting mechanism [139]. Li added Al_2O_3 and Fe_3O_4 to paraffin wax to prepare NPCMs, and analyzed the melting and energy storage mechanisms inside the materials using ultrasonic and magnetic fields (Shown in Figure 11) [140]. Zhuang added Al_2O_3 and Fe_3O_4 to paraffin wax to prepare NPCMs, and analyzed the heat transfer mechanism of NPs to the materials by thermochromic liquid crystal combined with a magnetic field [141]. Farahani analyzed the effects of fin factors and Fe_3O_4 EMPs concentration on the thermal performance of energy storage systems under the application

of magnetic fields [142]. The main materials and research contents of the above-mentioned study are listed in Table 9.

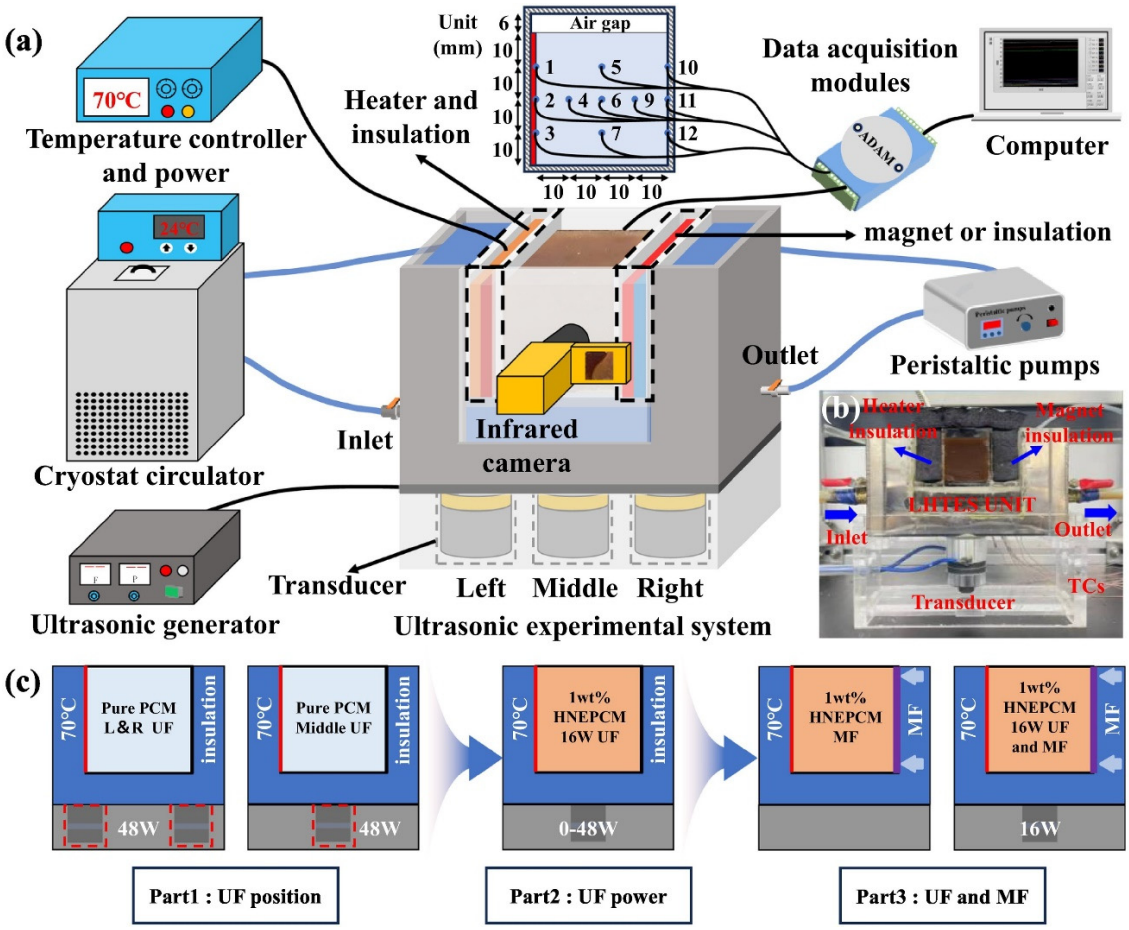

Figure 11. Ultrasonic experimental system diagram (Reproduced with permission from [140], Elsevier, 2024). (**a**) Schematic diagram; (**b**) experimental setup of the ultrasonic and magnetic fields experimental system; (**c**) Boundary conditions under different cases.

Table 9. The main materials and research contents about the magnetic field.

Reference	Materials	Physical Model	Initial and Boundary Conditions	Governing Equations	Approach	Key Parameters
Izadi et al. [132]	Al_2O_3, paraffin	Ahexagonal heat storage unit	$\theta(\hat{x},\hat{y},0)=0$, $\hat{u}(\hat{x},\hat{y},0)=\hat{v}(\hat{x},\hat{y},0)=0$; $\theta(\hat{x},\hat{y},\tau)=0$, $\hat{u}(\hat{x},\hat{y},\tau)=\hat{v}(\hat{x},\hat{y},\tau)=0$; $\frac{\partial\theta(\hat{x},\hat{y},\tau)}{\partial N}=0$, $\hat{u}(\hat{x},\hat{y},\tau)=\hat{v}(\hat{x},\hat{y},\tau)=0$.	Continuity, momentum in two coordinate directions and energy equations	The enthalpy-porosity method, the finite element method	The tilted angle and intensity of the magnetic field, the Hartmann number, Nu, the nanoadditives concentration
Hassan et al. [133]	Shell-core structured particles suspended in water	A U-shaped baffled cavity	$t=0, u=x=0$; $\theta_b=1$; $\theta_t=0$; $\frac{\partial\theta}{\partial n}=0$.	Continuity, momentum conservation with additional source terms, and energy balance	The Arbitrary Lagrangian–Eulerian approach, the deformation gradient tensor and the second Piola–Kirchhoff stress tensor	Rayleigh number, Stefan number, fusion temperature, NP volume fraction, oscillation amplitude, Young's modulus, Hartmann number, the variable time
Younis et al. [134]	A graphene core encapsulated by a polyurethane shell	A prism cover drive chamber	$\frac{\partial U}{\partial X}+\frac{\partial V}{\partial Y}=0$.	Continuity, momentum conservation, and energy balance	Galerkin method, Boussinesq approximation	Reynolds number, Darcy number, Darcy number, the angle of deflection

Table 9. *Cont.*

Reference	Materials	Physical Model	Initial and Boundary Conditions	Governing Equations	Approach	Key Parameters
Selimefendigil et al. [135]	Water-Ag-MgO hybrid NF	A triangular shape	-	Continuity, momentum conservation, and energy balance	Kozeny–Carmen model, method, the finite element method, Streamline Upwind Petrov–Galerkin approach, Biconjugate Gradient Stabilized	Port size, Reynolds number, Reynolds number.
Selimefendigil et al. [136]	Ag-MgO, paraffin	Multi jet impingement system	-	Energy equation, conservation equation.	finite element method, Lagrange FEs of various orders, SUPG, BICGStab. Kozeny–Carmen method	Nu, Reynolds number, magnetic field strength and inclination
Selimefendigil et al. [137]	Spherical Al_2O_3, cylindrical MWCNT, platelet GNP	Trapezoidal vented cavity	$u = u_g, T = T_g, T = T_h, \frac{\partial T}{\partial n} = 0.$	Continuity, momentum conservation, and energy balance	Kozeny–Carman model, Galerkin weighted residual finite element method	Reynolds number, Hartmann number, inclination parameter, non-uniform amplitude, NP loading.
Nguyen et al. [138]	Al_2O_3, paraffin	A closed fined rectangular chamber	$\theta = 0, U = V = 0 \forall F_0, X, Y \exists F_0 = 0;$ $\theta = 1, U = V = 0 \forall F_0, X, Y \exists 0 \leq X \leq 1, Y = 0; \theta = 1, U = V = 0 \forall F_0, X, Y \exists 0 \leq X \leq 1, Y = 1;$ $\frac{\partial \theta}{\partial \overline{x}} = 0, U = V = 0 \forall F_0, X, Y \exists X = 0, 0 \leq Y \leq 1;$ $\frac{\partial \theta}{\partial \overline{x}} = 0, U = V = 0 \forall F_0, X, Y \exists X = 1, 0 \leq Y \leq 1.$	Continuity, momentum conservation, and energy balance	The effective thermal conductivity of ferromagnetic-PCM, Boussinesq approximation	Capsule location, Hartmann number,
Lu et al. [139]	Fe_3O_4, paraffin	a glass beaker filled with PCM	-	-	uncertainty analysis	NP mass fraction, magnetic field rotational speed
Li et al. [140]	Al_2O_3, Fe_3O_4 acetylacetone	Ultrasonic experimental system	-	-	SEM, EDS, uncertainty analysis	Nu, filling height, melting time, melting rate
Zhuang et al. [141]	Al_2O_3, paraffin	A set of visualized experimental systems based on thermochromic liquid crystal (TLC)	-	-	TLC, GetData software Version 2.26, uncertainty analysis	Nu, filling height, melting time, melting rate
Farahani et al. [142]	RT82, Fe_3O_4.	Annular structure with strip fins	-	Continuity, momentum conservation, and energy balance	SIMPLE algorithm, center difference and quick method	Uniform magnetic field pattern, fin effect, melting time, NPs concentration.

4. Algorithm-Driven Optimization

Algorithm-driven optimization has become an important research strategy for enhancing the performance of NPCMs in high-temperature thermal storage systems [143]. This strategy utilizes the powerful computational capability of algorithms to finely optimize parameters such as the composition and structural design of NPCM, in pursuit of maximizing thermal efficiency and thermal stability. In the NPCM field, algorithms play a critical role in determining the ideal mass ratio of the base PCMs to NPs. They filter optimal solutions from numerous combinations of NP characteristics and PCM properties based on preset material performance benchmarks, which may encompass multiple dimensions ranging from maximizing thermal conductivity and energy storage capacity to enhancing thermal and electrical efficiency [144]. Furthermore, algorithm-driven optimization extends to the manufacturing processes of NPCM. During the synthesis of composite materials, algorithms take into account parameters such as mixing intensity, temperature regulation, and pressure control. By optimizing these factors, it is possible to enhance the performance of NPCM while also reducing costs, making NPCM more attractive for large-scale applications in high-temperature thermal storage and thus promoting the development of more efficient and sustainable energy solutions [145].

4.1. Machine Learning Methods

Machine learning methods serve as a system analysis and prediction paradigm based on the inherent laws of massive data. By deeply mining the hidden correlations within complex systems, these methods break through the simplification dependence of traditional physical models on complex boundary conditions and multi-field coupling mechanisms. In the thermal performance study of NPCMs, this approach demonstrates significant advantages: through high-dimensional data analysis of the synergistic effects of multiple parameters, it can accurately capture the distribution of NPs, the evolution of phase change interfaces, and the nonlinear response patterns of flow within porous media, revealing cross-scale coupling mechanisms that are difficult to quantify with traditional theoretical models. This data-centric research paradigm not only optimizes the thermal management performance prediction of nano PCM in complex geometric structures but also provides a new pathway for the intelligent design of industrial-grade phase change energy storage systems. The following is an overview of the research on the application of the latest machine learning methods to the analysis of NPCM.

Shakibi uses CFD simulation to design key factors, construct an Artificial neural network (ANN) model (Shown in Figure 12), and integrate long short-term memory (LSTM), grey wolf optimizer (GWO), Particle swarm optimization (PSO) and other methods to analyze and solve the intelligent model of the optimal thermal performance parameters [146]. Aly explored the heat and mass transfer properties of NPCM in a wave porous cavity using the incompressible smoothed particle hydrodynamics method and the extreme gradient boosting (XGBoost) machine learning model, Darcy number, Rayleigh number, Fusion temperature, Soret number, Dufour number, Hot zone length, Hot zone Key parameters such as height reveal the influencing characteristics of internal thermal performance [147]. Abdolahimoghamad established the multilayer perceptron (MLP)-ANN model for estimating the optimal melting and solidification time of Gr-Cu hybrid NPs and latent heat, thermal conductivity of bio-based NPCMs [148,149]. Gao established an automatic correlation determination model to predict liquid-state thermal conductivity, k-nearest neighbor and polynomial regression composite models to predict the thermal conductivity of NPCMs, and minimum absolute shrinkage and choice operators to predict freezing-state latent heat [150]. Ghasemi established an ANN model and input heat flux, Reynolds number, and concentration to predict performance evaluation criterion and average Nu [151]. Kiaghadi used four models: linear regression, lasso regression, polynomial regression, and auto-regressive integrated moving average to verify the correlation between time and liquid fraction, and confirmed that the data analysis method can be effectively applied to the prediction of phase transition behavior [152]. The auto-regressive integrated moving average algorithm was used to predict parameters such as solar unit time, PV temperature, melting fraction, NPCM temperature, electrical efficiency, and other parameters based on historical data [153]. Yang established an ANN model with Reynolds number and porosity of nickel foam as inputs, which could effectively predict the maximum temperature of LIB [154]. Xu established an ANN model with shear rate and mass fraction as inputs, which could effectively predict the dynamic viscosity, density, and shear stress of the LIB of the NPCM [155]. Salari established a Harris Hawks optimizer model optimized by a random forest algorithm to predict printed circuit board (PCB) temperature [156]. Khadem established a GWO-support vector regression with a hybrid composite model (Shown in Figure 13), and predicted the chipset temperature parameters through the melting point, thermal conductivity, specific heat capacity, and enthalpy parameters of the system [157]. Fini developed a composite model of an ANN-multiobjective genetic algorithm for predicting the Nu and pressure drop of microencapsulated PCM fluid [158]. The main materials and research contents of the above-mentioned study are listed in Table 10.

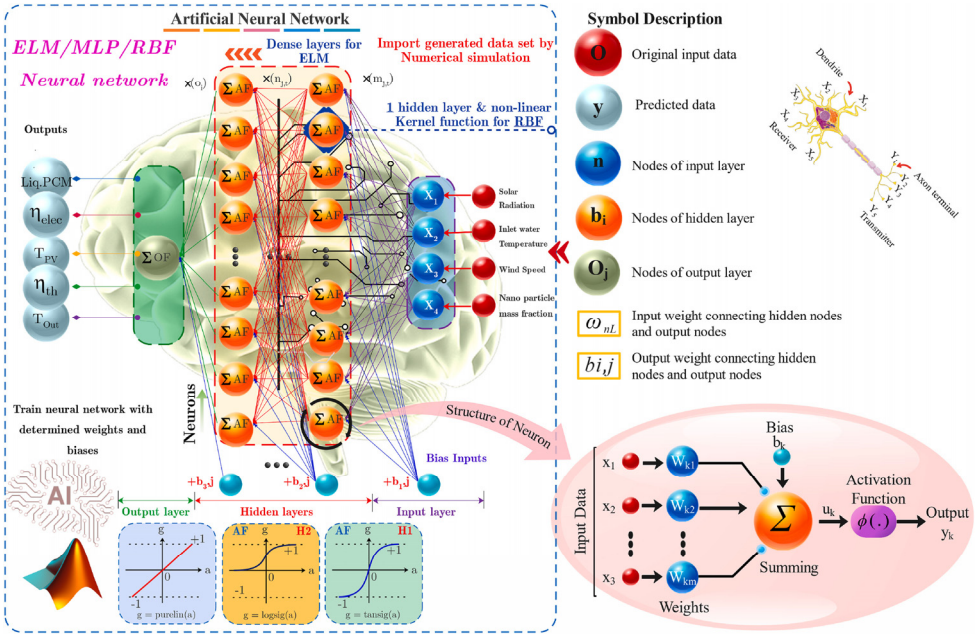

Figure 12. Schematic diagram of machine learning model (Reproduced with permission from [146], Elsevier, 2023).

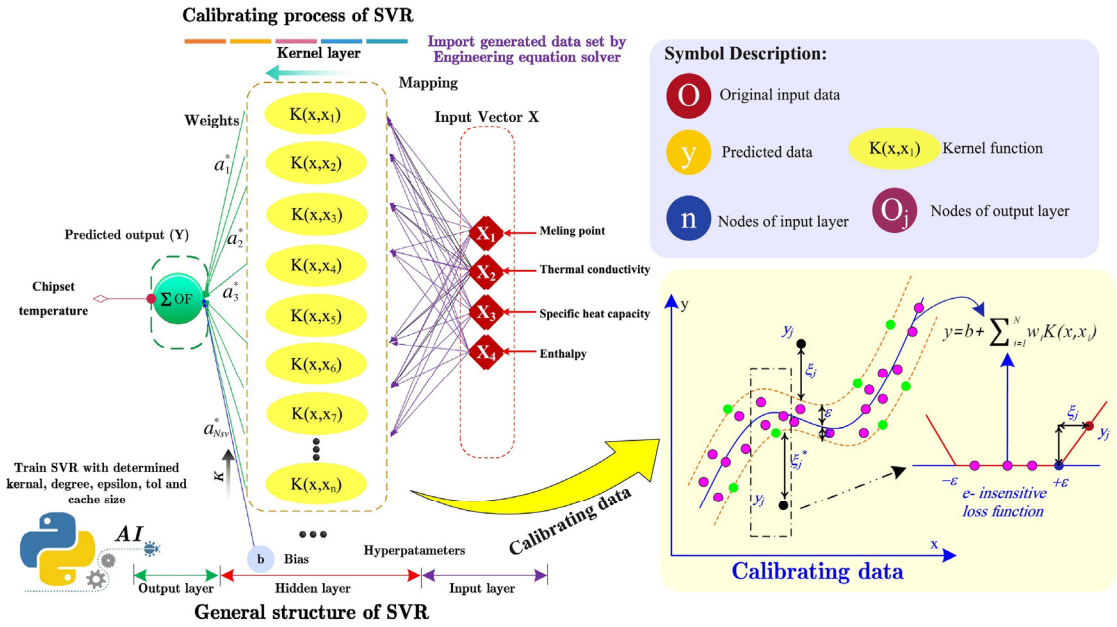

Figure 13. Support vector regression with hybrid model (Reproduced with permission from [157], Elsevier, 2023).

Table 10. The main materials and research contents about the machine learning methods.

Reference	Materials	Model	A pproach	Input	Output	Mean Absolute Percentage Error
Shakibi et al. [146]	MWCNT/PCM	ANN	CFD, LSTM, Extreme Learning Machine, Radial basis function, MLP, GWO, bat algorithm (BA), optimization based on biogeography (BBO), PSO, TOPSIS, LINMAP, and Shannon entropy	Surface temperature, coolant outlet temperature, electrical efficiency, thermal performance, melted PCM	Surface temperature, coolant outlet temperature, electrical efficiency, thermal performance, melted PCM	PSO: 0.09714; BBO: 0.07890; GWO: 0.07800; BA: 0.07837

Table 10. *Cont.*

Reference	Materials	Model	A pproach	Input	Output	Mean Absolute Percentage Error
Aly et al. [147]	PMMA, n-octadecane, water	XGBoost	the least squares boosting method	Nu, Sherwood number	Nu, Sherwood number (SH)	Nu: 5×10^{-7}; SH: 2.1×10^{-7}
Abdolahimoghadam et al. [148]	Beeswax, coconut oil, Gr-Cu hybrid NPs	MLP-ANN	Tansig, radbas	Temperatures, concentrations, thermal conductivity, liquid or solid state of PCM, latent heat of melting and solidification processes	Latent heat, thermal conductivity	TC: 1.1253×10^{-4} Latent heat: 4.7×10^{-4}
Abdolahimoghadam et al. [149]	Beeswax, coconut oil, Gr-Cu hybrid NPs	MLP-ANN	Trainlm, trainbr, tansig, radbas, logsig	Concentration, density, average temperature, specific heat, viscosity, latent heat, thermal conductivity	The melting's and solidification's liquid fraction and time,	Solidification: 6.1019×10^{-7}, 0.0458; Melting: 8.05×10^{-5}, 0.00935
Gao et al. [150]	MWCNT, GNPs, nano-graphite (NG), myristic acid (MA)	Automatic correlation determination; k nearest neighbors and polynomial regression; Minimum absolute shrink and selection operators	-	Solid-state thermal conductivity; thermal conductivity of pure myristic acid, temperature; Melting-state latent heat	Liquid-state thermal conductivity; thermal conductivity of NPCMs; Freezing-state latent heat	GNPs/MA: 1.762×10^{-4}; MWCNTs/MA: 5.45×10^{-7}; NG/MA: 5.035×10^{-6}
Ghasemi et al. [151]	Al, microencapsulated PCM-37	ANN	Levenberg-Marquardt, sigmoid, backpropagation algorithm, Regularization techniques	Heat flux, Reynolds number, concentration	Performance evaluation criterion, average Nu	-
Kiaghadi et al. [152]	RT44HC, Silver	Auto-regressive integrated moving average	Linear regression, lasso regression, polynomial regression	Time	Liquid fraction	0.0093
Kiaghadi et al. [153]	RT28HC, Cu	Auto-regressive integrated moving average	Linear regression, lasso regression, polynomial regression	Time, temperature of PV, melting fraction, temperature of NPCM, electrical efficiency	Time, temperature of PV, melting fraction, temperature of NPCM, electrical efficiency	-
Yang et al. [154]	$LiFeO_4$, n-nonadecane sodium lauryl sulfate, n-eicosane	ANN	ReLU	Reynolds number, porosity of nickel foam	Maximum temperature	-
Xu et al. [155]		ANN	Gradient descent algorithm	Shear rate and mass fraction	Dynamic viscosity, density, shear stress	0.00066
Salari et al. [156]	MWCNT, RT-35 HC, RT-47	Harris Hawks optimizer	Random forest	-	The temperature of PCB	-
Khadem et al. [157]	RT-35 HC, aluminum foam	Support vector regression with hybrid	GWO	Meling point, thermal conductivity, specific heat capacity, enthalpy	Chipset temperature	-
Fini et al. [158]	n-Octadecane, Polymethyl methacrylate	ANN-multiobjective genetic algorithm	NSGA-II, LINMAP, TOPIS, Shannon Entropy	Reynolds number, volume fraction	Nu, pressure drop	-

Monte Carlo methods, which often conduct research by leveraging the Bayesian approach optimized by Markov chain Monte Carlo, play a crucial role. Regarding data processing, the distribution of independent variables, such as normal distribution or log-normal distribution, is set according to different scenarios, and the corresponding dependent variables are determined [159]. Multiple models are established, and a large amount of input—output data is utilized, with the training set and the test set divided in a specific proportion, and metrics such as mean squared error, root mean squared error, and coefficient of determination are employed to analyze the prediction accuracy of the models [160]. Some studies also use the mean value, the standard deviation of the number of iterations, and the standard deviation for precise data analysis. In the research on the dispersion of highly conductive nanomaterials in D-mannitol to enhance heat transfer in the LHTES system, parameters related to the thermophysical properties of NPCM and the inlet conditions of the heat-conducting fluid are set as independent variables following a normal distribution, with the Fourier number (Fo) as the dependent variable. Based on 153 CFD data, four models are established by dividing the training set and the test set into an 8:2 ratio. The curves of the Fo values predicted and the actual Fo values by the four

models are shown in Figure 14. Eventually, a model that can best predict the Fo of the actual dataset is constructed based on relevant metrics [161]. In the study of graphite nanosheets reinforcing dodecanol ($C_{12}H_{26}O$), the melting rate and the surface-average Nu are set as independent variables with a normal or log-normal distribution, and the Stefan number, Grashof number, and Fo are set as dependent variables. Based on 573 melting-rate datasets and 516 surface-average Nu-number datasets, five models are established by dividing the training set and the test set in a 7:3 ratio. Subsequently, the models that can best predict the dataset values and the Nu values are analyzed, fully demonstrating the application of the Monte Carlo method in practical research [162]. The main materials and research contents of the above-mentioned study are listed in Table 11.

Table 11. The main materials and research contents about the Monte Carlo Method.

Ref.	Materials Set-Up	Analysis Method
Alazwari et al. [161]	Highly conductive nanomaterials dispersed in D-mannitol can be utilized to enhance heat transfer in LHTES systems	The Bayesian method optimized by Markov chain Monte Carlo is implemented. Independent variables (normally distributed): TC, density, specific heat capacity of the thermophysical properties of NPCM, as well as Reynolds number and inlet temperature of the inlet conditions of the heat conducting fluid. Dependent variable: Fo. Data analysis: Four models are established with 153 input-output CFD data. The ratio of the training set to the test set is 8:2. Mean Squared Error, Root Mean Squared Error, and Coefficient of Determination (R^2) are used to analyze the accuracy of the model's predicted values. A model that can best predict the Fo of the actual dataset is established to predict the dimensionless melting time.
Goodarzi et al. [162]	Graphite nanosheets reinforcing dodecanol ($C_{12}H_{26}O$)	The Bayesian method optimized by Markov Chain Monte Carlo is implemented. Independent variables (normally distributed or log-normally distributed): Melting rate and surface-average Nu. Dependent variables: The Stefan number, which is the ratio of sensible heat to latent heat and represents the driving force for melting. The Grashof number indicates the intensity of natural convection of liquid PCM during the melting process. Finally, the Fo represents the dimensionless time in transient problems. The model that can best predict the dataset values was analyzed. Another model that can best predict the Nu values was analyzed. Data analysis: Five models are established, using 573 melting-rate datasets and 516 surface-average Nu-number datasets. The ratio of the training set to the test set is 7:3. The mean, the standard deviation of the number of iterations, and the standard deviation are used for precise data analysis. The coefficient of determination, root-mean-squared error, and mean-squared error are used to evaluate the accuracy of the predicted values of the proposed models.

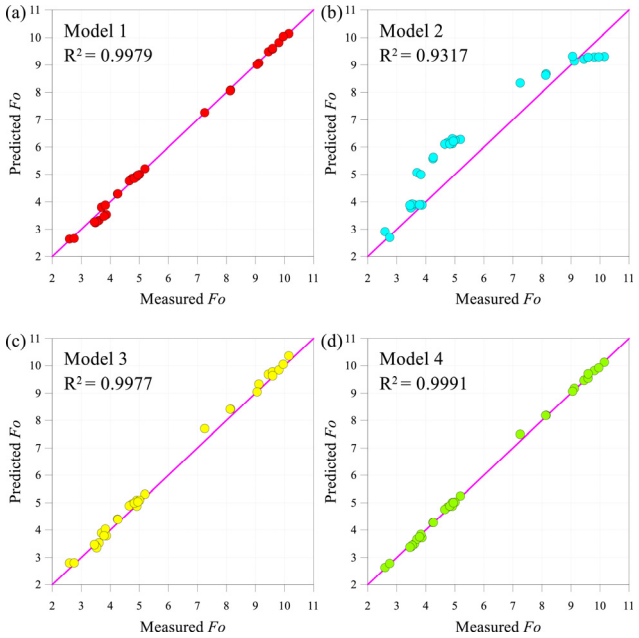

Figure 14. The curves of the Fo values by the four models (Reproduced with permission from [161], Elsevier, 2022). (**a**) Model 1; (**b**) Model 2; (**c**) Model 3; (**d**) Model 4.

4.2. Uncertainty Quantification Techniques

The uncertainty quantification techniques are uncertain to comprehensively assess the impact of uncertainty factors in systems on outcomes [163]. By meticulously identifying and precisely quantifying various sources of uncertainty, including measurement errors, model assumptions, and parameter variability, they provide strong assurance for the accuracy and reliability of models, enabling effective improvements on this basis [164]. In many fields, uncertainty quantification techniques play a crucial role, particularly in the research and application of complex systems based on NPCM materials. They assist researchers in gaining a deeper understanding of the intrinsic uncertainty mechanisms within the system, thereby allowing for a full consideration of uncertainty factors in model construction, optimization, and decision-making processes, ensuring the scientific and rational nature of the results. The following is an overview of the research on the application of the latest uncertainty quantification techniques to the analysis of NPCM.

Al-Aasam calculated that the error value of the PVT system caused by temperature, mass glow rate, solar irradiance, voltage, and current is 3.83% [165]. Daneshazarian determined that the error value of the ground source heat pump system resulting from temperature outlet, temperature inlet, and flow rate is 0.5% [166]. Gür analyzed the error value of the electronics system attributed to the temperatures of the PCM and the temperatures of the empty system, which is 1.5% [167]. Venkatesh conducted an analysis of the error in the heat exchanger system using parameters of radiation, temperature, wind velocity, and flow rate [168]. Ganeshkumar examined the error values of parameters such as mass flow rate, Nu, Convective heat transfer coefficient (CHTC), heat gain, solar energy, and energy efficiency for the solar air heater [169]. Amin adopted the Holman method to calculate the error values caused by solar radiation, temperature, and productivity in the freshwater production system, which were ±1.55%, ±1.2%, and ±1.58%, respectively [120]. Singh analyzed that the total error of the thermal performance system of solar ponds using NPCM was 2.59% [121]. Al-Karboly integrated the design of the photovoltaic system and analyzed that the total error caused by sensors or instruments was less than 4% [123]. Bassam utilized SiC and water to prepare nanofluids, and SiC and paraffin to prepare NPCMs, comprehensively designed photovoltaic systems, and analyzed the error values

caused by temperature, radiation, voltage, and flow measurements [127,128]. The main materials and research contents of the above-mentioned study are listed in Table 12.

Table 12. The main materials and research contents about uncertainty quantification techniques.

Reference	Materials	System	Parameters	Total Uncertainty (%)
Al-Aasam et al. [165]	SiC, paraffin	PVT	Temperature, mass glow rate, solar irradiance, voltage and current	3.83
Daneshazarian et al. [166]	Ag, Cu, Al_2O_3, CuO, TiO_2, GNP, MWCNT, paraffin	Ground source heat pump	Temperature outlet, temperature inlet, flow rate	0.5
Gür et al. [167]	Y_2O_3, myristic acid	Electronics	The temperatures of PCM, the temperatures of empty system	1.5
Venkatesh et al. [168]	SiC, Ag, paraffin	Heat exchanger	Radiation, temperature, wind velocity, flow rate	-
GaneshKumar et al. [169]	Al_2O_3, paraffin	Solar air heater	Mass flow rate; Nu; CHTC; heat gain; solar energy; energy efficiency	±2.5; ±3.9; ±4.1; ±4.32; ±5.45; ±4.21
Amin et al. [120]	Graphene, beeswax	Freshwater production	Intensity of solar radiation, temperature, productivity	±2; ±0.1; ±5
Singh et al. [121]	Al_2O_3, OM-37	Solar ponds	Magnetic stirrer, weight of NP and PCM, thermal analysis in DSC, hot disk thermal constants analyzer, solar intensity, wind speed, temperature	2.59
Al-Karboly et al. [123]	SiC	PV	temperature, mass flow rate, solar irradiance, voltage and current.	3.82
Bassam et al. [127,128]	SiC, paraffin	PV	Temperature, radiation, voltage, flow	±0.1; ±1.5; ±1.0; ±0.5

5. Techno-Economic Analysis

The techno-economic analysis within the framework of NPCM is a comprehensive evaluation that combines considerations of both technological and economic feasibility [170]. This analysis delves deeply into the specifics of NPCM-related technologies, exploring everything from fundamental scientific principles to practical applications, and accurately assesses the costs and potential benefits associated with research and development, production, and maintenance. It not only predicts short-term financial impacts but also evaluates long-term economic sustainability. By integrating technological and economic dimensions, techno-economic analysis provides stakeholders with a holistic view, assisting them in making informed investment decisions in NPCM projects and ensuring the efficient allocation of resources in this emerging field [171].

5.1. Cost-Benefit Analysis

Cost-benefit analysis is a systematic decision-making tool, the core logic of which lies in quantifying and comparing all expected costs and benefits of an NPCM product over its entire lifecycle, while considering the time value of the product [172,173]. Ultimately, it calculates key indicators to evaluate the economic feasibility of the product as well as the relative advantages of different proposals [174]. For NPCM products, cost-benefit analysis effectively avoids resource waste by preemptively identifying projects where expected benefits will not cover costs, thus preventing the allocation of valuable funds to inherently unprofitable innovations. Furthermore, in the context of limited resources, it optimizes resource allocation by horizontally comparing the net benefit priorities of various NPCM proposals, ensuring investments are directed towards the avenues with the highest economic potential. This transforms innovation risks into measurable investment propositions, maximizing the likelihood of creating long-term value [175]. The following is

an overview of the research on the application of the latest cost-benefit analysis method to the analysis of NPCM.

Sharshir analyzed that the hemispherical solar still device with metal organic framework is the most cost-effective and efficient, with the highest unit production cost and life cycle cost for producing fresh water [176]. Rasaiah studied multiple nanofluid improved double slope solar still devices and found that CuO nanofluid has the highest cost-effectiveness in terms of economy and environmental protection [177]. Kumar's study found that the configuration of aluminum foam and PCM with microchannels helps maintain efficient flow conditions but has higher maintenance costs [178]. Gürbüz designed a collector embedded with S NPs and analyzed it from multiple perspectives, such as efficiency, energy, and cost [179]. Mohtasim studied the energy recovery period and economic and environmental factors, such as CO_2 reduction of solar still systems and PVT systems with different structures [180]. Singh combined multiple NPCMs, the configuration of the device, and the analysis of daily freshwater production and investment payback period parameters under various conditions were carried out [181]. Anika comprehensively analyzed the performance, economy, environment, and other factors of the distiller constructed with mixed NPCMs and proposed improvement suggestions [182]. Rad designed a PVT system using nanofluid as a coolant and found that the unit production cost was 0.134 $/kWh [183]. Essa placed PCM and Ag NPs under the absorber to design the best-performing solar still, and the research results showed that the use of the device increased freshwater productivity by 245% [184]. Paul regarded different NPs as important factors affecting the thermal and environmental economic performance of the solar distiller [185]. Elamy combined Ag NPs for comprehensive solar still research; the results showed that the productivity of the slipped material increased by 233%, and both the environmental and economic cost-effectiveness were improved [186]. Attia's work demonstrated that incorporating graphene materials into the design of solar stills led to a remarkable 574.1% enhancement in energy efficiency [187]. El-Gazar combined the characteristics of TiO_2 and SiO_2 to design a solar still system and found that the production cost of distilled water was lower in summer than in winter [188]. The main materials and research contents of the above-mentioned study are listed in Table 13.

Table 13. The main materials and research contents about cost-benefit analysis.

System	Product	Unit Production Cost	Life Cycle Cost	Payback Period	CO_2 Reduction	Ref.
Solar still	Distilled water	0.0115 $/L	130 $	-	1.57 ton/year	[176]
Solar still	Distilled water	0.09 $/L	219 $	496 days	16.80 ton/payback period	[177]
Battery	Flow condition	-	49–70 $	-	-	[178]
Collector	Electrical energy	0.0138 €/kWh	3.6624 €	0.058 year	-	[179]
Solar still/PVT	Distilled water; electrical energy	0.01495 $/L	-	7.263 year; 0.26 year	3322.12 kg (emissions), 564.82 kg (mitigation); 6.98 ton/payback period	[180]
Solar still	Distilled water	0.012 $/L	-	129 days	-	[181]
Solar still	Distilled water	0.0192 $/L	-	7.26 year	322.12 kg (emissions); 565 kg (mitigation)	[182]
PVT	Electrical energy	0.134 $/kWh	-	-	-	[183]
Solar still	Distilled water	0.011 $/L	-	-	-	[184]
Solar still	Distilled water	-	-	-	448 kg/m^2 year	[185]
Solar still	Distilled water	0.01 $/L		420 days	28.8 ton/year	[186]
Solar still	Distilled water	0.00713 $/L	65.85$	-	-	[187]
Solar still	Distilled water	0.0156 $/L (in summer), 0.0264 $/L (in winter)	-	-	16.38 ton/year (in summer), 19.47 ton/year (in winter)	[188]

After delving into a series of cases where the latest cost-benefit analysis method was applied to NPCM analysis, the remarkable practical advantages and potential of this

method are evident. These cases span multiple industries like freshwater, photovoltaic, and electric power, and involve complex NPCM scenarios. They offer decision-makers clear, intuitive, and actionable references. This approach effectively overcomes the blind spots and limitations of conventional analysis. By applying it, businesses can optimize resource allocation in NPCM implementation. This, in turn, enhances economic efficiency while advancing sustainable development goals.

5.2. Policy Incentives and Market Growth Potential

Policy incentives are constructing a multi-level environmental governance system, driving the global green transition. Under the UN framework, conference of the parties (COP) 29 established the climate finance target, mandating developed countries to provide $300 billion annually in public funds by 2035 to leverage $1.3 trillion in support for developing countries' infrastructure development [189]; COP30 proposes establishing a carbon tariff revenue-sharing mechanism and a deforestation accountability mechanism to ensure biofuel and mineral development do not harm the ecological rights of developing countries [190]. At the international institutional level, the International Energy Agency (IEA) demonstrated through its Strategy for an Affordable and Fair Clean Energy Transition that renewable energy costs are lower than fossil fuels [191], and its 2023 Energy Efficiency Report requires doubling the global annual energy efficiency improvement rate to 4% by 2030 [192]; the tripling renewable energy capacity target (to 11.2 TW by 2030) jointly advanced by the IEA and International Renewable Energy Agency (IRENA) has shown tangible results that China contributed 64% of the 585 GW global new installations in 2024 [193]. The EU established a 40% minimum domestic clean energy production capacity target by 2030 through its Net Zero Industry Act [194], complemented by the Batteries and Waste Batteries Regulation mandating full lifecycle carbon footprint disclosure (implementing a battery passport by 2027) [195], combined with the Carbon Border Adjustment Mechanism imposing comprehensive tariffs on six high-carbon import sectors [196]. Supported by the Critical Raw Materials Act aiming to increase strategic raw material processing to 40% and recycling rates to 25% [197], and augmented by the EU Wind Power Action Plan streamlining permitting processes (targeting 120 GW for North Sea wind power by 2030) [198], this forms a tripartite "technological autonomy-supply chain decarbonization-resource circularity" system. The US revised the Inflation Reduction Act, raising clean electricity tax credits to 35% (with domestic manufacturing requirements) and removing battery mineral restrictions [199], while New York State enacted the Climate Change Superfund Act, imposing a $75 billion levy on fossil fuel companies [200]. Developing countries are advancing concurrently: China's Energy Law established a renewable energy consumption guarantee mechanism and initiated a unified energy market [201], while its Draft Ecological Environment Code consolidated over 30 laws to create a dedicated "Green and Low-Carbon" chapter [202]; India launched a national carbon market covering power and petrochemical sectors, paired with a 280 GW solar target [203]; Vietnam's Revised Electricity Law introduced direct green power purchase agreements exempting them from bidding [204]; Brazil invested R$21 billion in its National Hydrogen Program [205]; the UAE's National Biofuel Policy established production standards promoting waste cooking oil conversion, targeting a 20% increase in biodiesel consumption by 2050 [206]. These policies, relying on mandatory fund allocation, technical standards, market mechanism restructuring, and ecological rights protection, transform global environmental commitments into enforceable binding rules, highlighting the critical role of policy-driven approaches in environmental governance. The main research contents of the above-mentioned study are listed in Table 14.

Table 14. The main research content about policy.

Policy/Legislation Name	Country/Region	Effective/Revised Date	Core Content	Ref.
New Collective Quantified Goal on Climate Finance	UN (COP29)	Nov 2024	Requires developed countries to provide $300 billion in public funding annually by 2035, mobilizing $1.3 trillion annually to support developing countries.	[189]
-	UN (COP30)	-	A carbon tariff revenue-sharing and deforestation accountability mechanism; Biofuel production and mineral extraction do not sacrifice the ecological rights of developing countries.	[190]
Strategies for Affordable and Fair Clean Energy Transitions	IEA	May 2024	Argues clean energy costs less than fossil fuels; proposes energy efficiency subsidies, promotion of efficient appliances, and clean transport.	[191]
2023 Energy Efficiency Report	IEA	Nov 2023	Requires doubling the global annual energy efficiency improvement rate to 4% by 2030.	[192]
Renewable Energy Capacity Tripling Goal	IEA/IRENA	2023–2025 (Progress)	Global renewable energy capacity to reach 11.2 TW by 2030; 585 GW added in 2024 (China accounted for 64%).	[193]
Net Zero Industry Act	EU	2025 (Implementation)	Local net-zero tech production capacity $\geq$40% by 2030; limits dependence on any single third country to >50%.	[194]
Batteries and Waste Batteries Regulation	EU	Feb 2025	Mandates disclosure of full-lifecycle carbon footprint for batteries; implements "battery passport" from 2027.	[195]
Carbon Border Adjustment Mechanism	EU	1 January 2025	Full carbon tax implementation on imports across six sectors (steel, Al, etc.).	[196]
Critical Raw Materials Act	EU	2023 (Adopted)	By 2030: 10% domestic extraction, 40% domestic processing, and 25% domestic recycling capacity for strategic raw materials.	[197]
European Wind Power Action Plan	EU	Oct 2023	Simplifies wind permitting; targets 120 GW North Sea offshore wind capacity by 2030.	[198]
Inflation Reduction Act Amendments	USA	2025 (Revision)	Raises clean electricity tax credit to 35% (requires domestic manufacturing); removes battery mineral "Foreign Entity of Concern" restrictions.	[199]
Climate Change Superfund Act	USA	2025	New York State to levy $75 billion over 25 years on fossil fuel companies.	[200]
Energy Law of the People's Republic of China	China	1 January 2025	Establishes renewable energy consumption guarantee; defines financial energy attributes; builds a unified energy market.	[201]
Ecological and Environmental Code (Draft)	China	Apr 2025 (Review)	Consolidates over 30 environmental laws; first-ever "Green and Low-Carbon Development" chapter.	[202]
National Carbon Market	India	Apr 2025 (Launch)	Covers power and petrochemical sectors; coupled with 280 GW solar PV target.	[203]

Table 14. *Cont.*

Policy/Legislation Name	Country/Region	Effective/Revised Date	Core Content	Ref.
Revised Electricity Law	Vietnam	1 February 2025	Introduces Direct Power Purchase Agreements, allowing green projects to bypass bidding.	[204]
National Hydrogen Program	Brazil	2023–2025	Invests BRL 21 billion; aims to establish a low-carbon hydrogen industrial chain by 2030.	[205]
National Biofuels Policy	UAE	Apr 2024 (Approved)	Sets biofuel production standards and trading rules; targets 20% increase in biodiesel consumption by 2050; promotes waste cooking oil conversion to biofuel.	[206]

6. Conclusions and Future Work

This review comprehensively analyzes NPCM's high thermal performance research methods and economic benefits, delves into its melting mechanisms, and optimal design configurations. Starting with the fundamental types of NPCM, it offers in-depth explanations of these mechanisms and designs, highlighting their advantages in thermal energy management. The review also incorporates cost-benefit analyses of application systems and the latest international environmental policies to fully assess NPCM's energy-saving and eco-friendly attributes. These findings demonstrate NPCM's great potential in materials innovation and low-carbon environmental protection, strongly supporting sustainable development.

6.1. Key Findings and Contributions

(1) NPCMs improve thermal conductivity, reduce supercooling, and accelerate melting/solidification rates.
(2) Various NPCM structures, such as thermophysical, photonic, fluid-based, encapsulated, and phase-engineered, enable targeted applications across different solar thermal systems.
(3) Mechanism-level analysis using MD and DFT provides critical insights into nanoparticle-PCM interactions and nano-scale heat transfer behavior.
(4) Techno-economic analyses confirm that NPCMs offer high cost-effectiveness, improved energy efficiency, and extended lifecycle benefits for solar energy systems.
(5) The identical Cu NPs and paraffin-based NPCM structure exhibit analogous thermal property inflection points at significantly disparate Cu NP concentrations. Consequently, it is imperative to establish a rigorous simulation model to analyze the correlation between nanoparticle concentration and the thermal performance characteristics of NPCM.
(6) The unit production cost of distilled water for solar distillers using NPCM can be as low as $0.00713/L, and other models of solar distillers also demonstrate good, low-carbon, and environmentally friendly economic performance.
(7) The combined use of mechanistic analysis methods and simulation methods is more conducive to studying the phase change mechanism of NPCM during the melting process.
(8) The combination of a finite element analysis model and experimental data is more advantageous for the analysis of the melting phase transition mechanism of NPCM under the action of a magnetic field.
(9) The application of algorithm optimization and analysis methods, particularly integrated algorithmic models based on artificial neural networks (ANNs), can be

harnessed to more effectively project the material configurations of devices or systems that achieve high thermal efficiency performance.

(10) The incorporation of graphene materials significantly enhances the performance characteristics of PCMs. For instance, in solar still applications, it improves energy efficiency by 574.1%. Therefore, graphene and other high-performance materials should be prioritized in future NPCM research.

(11) Increasing policy incentives, clean energy mandates, and investments in renewable infrastructure are accelerating the commercial potential of NPCM-based solutions.

6.2. Remaining Challenges and Future Opportunities

Although NPCM exhibits strong thermal performance in melt heat transfer, the design and selection of its nano materials or structures face challenges in practical applications. As different researchers have discussed NPCM from various research perspectives, integrating innovative research ideas into the design of NPCM application systems has become a mainstream research direction. Research on NPCM holds extensive promise, and future leading research methods are likely to be associated with it.

(1) The accuracy of ideal model simulation methods, which is related to mesh size, models, quantities, and solution methods, necessitates further research to design high-precision physical simulation models and reduce interference from inaccuracies in real-world models.

(2) In algorithm optimization analysis, which demands extensive data collection with accuracy being critical, the impact of varying parameter choices in different algorithms on model outcomes necessitates further exploration into constructing high-quality datasets and developing efficient, accurate algorithmic models.

(3) During the experiment, the inaccuracy caused by measuring devices is inevitable, highlighting the necessity for more precise system accuracy control and making it necessary to conduct uncertainty analysis on key steps.

(4) In actual solar energy system applications, unforeseen circumstances often arise during operation, so future research could integrate simulations of additional weather factors to develop a more realistic and production-oriented simulation model.

(5) An intelligent optimization model for solar-powered freshwater production systems should be established, since the study of nanomaterials within a single system is limited in scope, failing to take into account the substitutability of materials and the acceptability of economic costs.

(6) Although significant progress has been made in the research of thermodynamic melting associated with magnetic field convection across various fields, it is necessary to further explore the economic benefits of these findings and address the insufficient studies on the impact of eddy current characteristics in magnetic fields on the thermal properties of materials.

Author Contributions: Conceptualization, J.W. and W.L.; methodology, W.L.; software, M.W.; validation, M.W., J.Y. and D.M.; formal analysis, W.L.; investigation, W.L. and M.W.; resources, J.Y.; data curation, W.L.; writing—original draft preparation, W.L. and J.W.; writing—review and editing, E.H. and J.W.; visualization, D.M.; supervision, J.W.; project administration, J.W.; funding acquisition, J.W. All authors have read and agreed to the published version of the manuscript.

Funding: This research received no external funding.

Data Availability Statement: No new data were created or analyzed in this study.

Conflicts of Interest: The authors declare no conflict of interest.

Abbreviations

ANN	Artificial neural network
BA	Bat algorithm
BBO	Optimization based on biogeography
BET	Brunauer–Emmett–Teller
CFD	Computational fluid dynamic
CHTC	Convective heat transfer coefficient
COP	Conference of the parties
DFT	Density functional theory
DHPD	$Na_2HPO_4 \cdot 12H_2O$
DSC	Differential scanning calorimetry
F	Furfural
FEA	Finite element analysis
Fo	Fourier number
FTIR	Fourier transform infrared spectroscopy
GNP	Graphene nanosheets
GWO	Grey wolf optimization
IEA	International energy agency
IRENA	International renewable energy agency
L	Liquid
LHTES	Latent heat thermal energy storage
LIB	Lithium-ion battery
LSTM	Long short-term memory
MA	Myristic acid
MD	Molecular dynamics
MLP	Multilayer perceptron
MWCNT	Multi-walled carbon nanotube
NG	Nano-graphite
Ni@C/C	The hierarchically porous carbon structure infiltrated with Ni@graphite
NP	Nanoparticle
NPCM	Nanoparticle-enhanced phase change material
Nu	Nusselt
ODA	Octadecanol
OM	Oleic-acid-modified
PCB	Printed circuit board
PCM	Phase change material
PSO	Particle swarm optimization
PV	Photovoltaic
PVT	Photovoltaic-thermal
R	Resorcinol
RBF	Radial basis function
S	Solid
SA	Silica aerogel
SEM	Scanning electron microscope
SIMPLE	Semi-implicit method for pressure linked equations
SH	Sherwood number
TC	Thermal conductivity
TEM	Transmission electron microscope
TGA	Thermogravimetric analysis
TLC	Thermochromic liquid crystal
VMTNS	Vermiculite nanosheets

XGBoost	Extreme gradient boosting
XPS	X–ray photoelectron spectroscopy
XRD	X–ray diffractometer

References

1. Wang, J.; Gullo, P.; Ramezani, H. Review on the trend of ultra-low-GWP working fluids for small-capacity vapour-compression systems. *Sustain. Energy Technol. Assess.* **2024**, *66*, 103803. [CrossRef]
2. Alizadeh, O. A review of ENSO teleconnections at present and under future global warming. *WIREs Clim. Change* **2024**, *15*, e861. [CrossRef]
3. Rodés-Guirao, H.R.a.L. Peak Global Population and Other Key Findings from the 2024 UN World Population Prospects. Available online: https://ourworldindata.org/un-population-2024-revision?weekend-reading-link-040824/ (accessed on 1 May 2025).
4. Ngagoum Ndalloka, Z.; Vijayakumar Nair, H.; Alpert, S.; Schmid, C. Solar photovoltaic recycling strategies. *Sol. Energy* **2024**, *270*, 112379. [CrossRef]
5. Yu, J.; Cheng, H.; Wang, Y.; He, C.; Zhou, B.; Liu, C.; Feng, Y. Multiple shearing-induced high alignment in polyethylene/graphene films for enhancing thermal conductivity and solar-thermal conversion performance. *Chem. Eng. J.* **2024**, *480*, 148062. [CrossRef]
6. Wang, J.; Hu, E.; Blazewicz, A.; Ezzat, A.W. Investigation on the long-term performance of solar thermal powered adsorption refrigeration system based on hourly accumulated daily cycles. *Heat Mass Transf.* **2021**, *57*, 361–375. [CrossRef]
7. Ali, F.H.; Al-Amir, Q.R.; Hamzah, H.K.; Alahmer, A. Unveiling the potential of solar cooling technologies for sustainable energy and environmental solutions. *Energy Convers. Manag.* **2024**, *321*, 119034. [CrossRef]
8. Wang, J.; Hu, E.; Blazewicz, A.; Ezzat, A.W. Simulation of accumulated performance of a solar thermal powered adsorption refrigeration system with daily climate conditions. *Energy* **2018**, *165*, 487–498. [CrossRef]
9. Kasaeian, A.; Nazari, N.S.; Masoumi, A.; Shabestari, S.T.; Jadidi, M.; Fereidooni, L.; Bidhendi, M.E. A review on phase change materials in different types of solar stills. *J. Energy Storage* **2024**, *99*, 113430. [CrossRef]
10. Wang, B.; Liu, Y.; Wang, D.; Song, C.; Fu, Z.; Zhang, C. A review of the photothermal-photovoltaic energy supply system for building in solar energy enrichment zones. *Renew. Sustain. Energy Rev.* **2024**, *191*, 114100. [CrossRef]
11. Pintaldi, S.; Perfumo, C.; Sethuvenkatraman, S.; White, S.; Rosengarten, G. A review of thermal energy storage technologies and control approaches for solar cooling. *Renew. Sustain. Energy Rev.* **2015**, *41*, 975–995. [CrossRef]
12. Suresh, C.; Saini, R.P. Review on solar thermal energy storage technologies and their geometrical configurations. *Int. J. Energy Res.* **2020**, *44*, 4163–4195. [CrossRef]
13. Carnie, J.-T.; Hardalupas, Y.; Sergis, A. Decarbonising building heating and cooling: Designing a novel, inter-seasonal latent heat storage system. *Renew. Sustain. Energy Rev.* **2024**, *189*, 113897. [CrossRef]
14. Zhang, X.; Yu, C.; Zhang, C. Advances in latent heat storage technology for electronic cooling. *Renew. Sustain. Energy Rev.* **2025**, *215*, 115614. [CrossRef]
15. Ou, S.; Wang, P.; Yang, S.; Su, H. Thermal characteristics and energy-saving research of P-PCM FinTwall in hot summer and cold winter regions. *Energy* **2025**, *329*, 136670. [CrossRef]
16. Karaağaç, M.O. Experimental investigation of a novel PCM-enhanced underfloor heating system for energy-efficient sustainable buildings. *Appl. Therm. Eng.* **2025**, *275*, 126891. [CrossRef]
17. Chen, X.; Su, Y.; Zhang, Y.; Shen, J.; Xu, X.; Wang, X.; Zhou, F. Performance of thermal management system based on PCM/forked liquid-cold plate for 18650 cylindrical battery. *J. Energy Storage* **2024**, *91*, 112071. [CrossRef]
18. Kurşun, B.; Balta, M.; Karabulut, K. Exploring the impact of inner and middle channel geometries on the melting rate of PCM-metal foam composition in a triplex tube heat exchanger. *Therm. Sci. Eng. Prog.* **2024**, *51*, 102621. [CrossRef]
19. Palaniappan, M.; El-Shafay, A.S.; Shanmugan, S. Improving heat retention properties of steeped M-shape basin solar distillers utilizing paraffin RT50-enhanced silver nanoparticles and Manihot esculenta extracts. *Desalination* **2024**, *586*, 117836. [CrossRef]
20. Gürbüz, H.; Demirtürk, S.; Akçay, H.; Topalcı, Ü. Experimental investigation on electrical power and thermal energy storage performance of a solar hybrid PV/T-PCM energy conversion system. *J. Build. Eng.* **2023**, *69*, 106271. [CrossRef]
21. Manikandan, S.; Muthuvairavan, G.; Samykano, M.; Natarajan, S.K. Numerical simulation of various PCM container configurations for solar dryer application. *J. Energy Storage* **2024**, *86*, 111294. [CrossRef]
22. Ji, C.; Liu, D.; Waqas, H.; Sun, S.-L.; Jalili, B.; Abdelmohimen, M.A.H. Melting performance of Molten Salt with nanoparticles in a novel triple tube with leaf-shaped fins. *Case Stud. Therm. Eng.* **2024**, *61*, 105063. [CrossRef]
23. Ma, T.; Li, Z.; Lv, K.; Chang, D.; Hu, W.; Zou, Y. Design and performance analysis of deep peak shaving scheme for thermal power units based on high-temperature molten salt heat storage system. *Energy* **2024**, *288*, 129557. [CrossRef]
24. Reddy, B.D.; Rahul, S.V.S.; Harish, R. Impact of fin number and nanoparticle size on molten salt NanoPCM melting in finned annular space. *J. Energy Storage* **2023**, *72*, 108705. [CrossRef]
25. Gui, X.; Wang, S.; Ding, L. Simulation study of a novel phase change cooling garment for electricians in a high-temperature environment. *Int. J. Refrig.* **2024**, *168*, 79–88. [CrossRef]

26. Anter, A.G.; Sultan, A.A.; Hegazi, A.A.; El Bouz, M.A. Thermal performance and energy saving using phase change materials (PCM) integrated in building walls. *J. Energy Storage* **2023**, *67*, 107568. [CrossRef]
27. Madurai Elavarasan, R.; Nadarajah, M.; Pugazhendhi, R.; Gangatharan, S. An experimental investigation on coalescing the potentiality of PCM, fins and water to achieve sturdy cooling effect on PV panels. *Appl. Energy* **2024**, *356*, 122371. [CrossRef]
28. Zhan, H.; Mahyuddin, N.; Sulaiman, R.; Khayatian, F. Phase change material (PCM) integrations into buildings in hot climates with simulation access for energy performance and thermal comfort: A review. *Constr. Build. Mater.* **2023**, *397*, 132312. [CrossRef]
29. Gado, M.G. Thermal management and heat transfer enhancement of electronic devices using integrative phase change material (PCM) and triply periodic minimal surface (TPMS) heat sinks. *Appl. Therm. Eng.* **2025**, *258*, 124504. [CrossRef]
30. Madurai Elavarasan, R.; Pugazhendhi, R.; Shafiq, S.; Gangatharan, S.; Nadarajah, M.; Shafiullah, G.M. Efficiency enhancement of PV panels with passive thermal management using PCM: An exhaustive review on materials, designs and effective techniques. *Appl. Energy* **2025**, *382*, 125217. [CrossRef]
31. Anya, B.; Mohammadpourfard, M.; Akkurt, G.G.; Mohammadi-Ivatloo, B. Exploring geothermal energy based systems: Review from basics to smart systems. *Renew. Sustain. Energy Rev.* **2025**, *210*, 115185. [CrossRef]
32. Suo, Y.; Tang, C.; Jia, Q.; Zhao, W. Influence of PCM configuration and optimization of PCM proportion on the thermal management of a prismatic battery with a combined PCM and air cooling structure. *J. Energy Storage* **2024**, *80*, 110340. [CrossRef]
33. Al-Amayreh, M.I.; Alahmer, A. Efficiency enhancement in direct thermal energy storage systems using dual phase change materials and nanoparticle additives. *Case Stud. Therm. Eng.* **2024**, *59*, 104577. [CrossRef]
34. Murali, G.; Ramani, P.; Murugan, M.; Elumalai, P.V.; Ranjan Goud, N.U.; Prabhakar, S. Improved solar still productivity using PCM and nano-PCM composites integerated energy storage. *Sci. Rep.* **2024**, *14*, 15609. [CrossRef]
35. Kazaz, O.; Abu-Nada, E. Thermal performance of nano-architected phase change energetic materials for a next-generation solar harvesting system. *Energy Convers. Manag.* **2025**, *327*, 119541. [CrossRef]
36. Ulker, N.; Bulut, H.; Demircan, G. Comparative study on the effect of surface-modified nanoparticles on PCM for solar energy applications. *J. Therm. Anal. Calorim.* **2024**, *149*, 12053–12070. [CrossRef]
37. Bestas, S.; Aktas, I.S.; Bayrak, F. A bibliometric and performance evaluation of nano-PCM-integrated photovoltaic panels: Energy, exergy, environmental and sustainability perspectives. *Renew. Energy* **2024**, *226*, 120383. [CrossRef]
38. Goel, V.; Dwivedi, A.; Kumar, R.; Kumar, R.; Pandey, A.K.; Chopra, K.; Tyagi, V.V. PCM-assisted energy storage systems for solar-thermal applications: Review of the associated problems and their mitigation strategies. *J. Energy Storage* **2023**, *69*, 107912. [CrossRef]
39. Abdolahimoghadam, M.; Rahimi, M. The effect of the number of tubes on the charging and discharging performances of a novel bio-nPCM within a vertical multi-tube TES system. *Energy* **2025**, *319*, 135010. [CrossRef]
40. Dhivagar, R.; Singh, P.K.; Nandhakumar, E. Synergistic effect of stearic acid/bismuth oxychloride/cupric oxide for thermal storage applications: Preparation, stability, rheological and thermophysical analysis. *Phys. Scr.* **2024**, *99*, 065039.
41. Azeez, H.L.; Ibrahim, A.; Ahmed, B.O.; Dol, S.S.; Al-Waeli, A.H.A.; Jaber, M. Experimental evaluation of a novel photovoltaic thermal System: Energy, economic, and exergy-based sustainability analysis. *Case Stud. Therm. Eng.* **2025**, *71*, 106167. [CrossRef]
42. Ahmed, B.O.; Ibrahim, A.; Azeez, H.L.; Dol, S.S.; Al-Waeli, A.H.A.; Jaber, M. Energy and exergy analysis of a newly designed photovoltaic thermal system featuring ribs, petal array, and coiled twisted tapes: Experimental analysis. *Case Stud. Therm. Eng.* **2024**, *63*, 105388. [CrossRef]
43. Maseer, M.M.; Ismail, F.B.; Kazem, H.A.; Hachim, D.M.; Al-Gburi, K.A.H.; Chaichan, M.T. Performance enhancement of photovoltaic/thermal collector semicircle absorber tubes using nanofluid and NPCM. *Renew. Energy* **2024**, *233*, 121152. [CrossRef]
44. Máñez-Espina, L.M.; Díaz-Rubio, A. Control of the local and nonlocal electromagnetic response in all-dielectric reconfigurable metasurfaces. *Phys. Rev. Appl.* **2024**, *22*, 054022. [CrossRef]
45. Sathishkumar, A.; Sundaram, P.; Prabakaran, R.; Kim, S.C. Graphene based fatty acid phase change material as an alternative to water: An experimental investigation on thermal energy storage characteristics. *Colloids Surf. A Physicochem. Eng. Asp.* **2025**, *715*, 136589. [CrossRef]
46. Baiju, V.; Priya, K.L.; Shafi, K.A.; Shahid, P.A.M.; Lamba, R.; Singh, H.; Ichiyanagi, M.; Suzuki, T.; Shajan, S. Enhanced latent heat storage for solar thermal applications using tapered fins and hybrid nano-additives. *J. Energy Storage* **2025**, *118*, 116308. [CrossRef]
47. Wu, Z.; Shao, Y.; Li, M.; Zou, M.; Wu, K.; Chen, W.; Huang, X.; Ma, C.; Ran, J. Stability and discharging performance improvements of modified nano particle enhanced binary alkanes capsule for cold latent heat storage tank. *J. Energy Storage* **2025**, *117*, 116169. [CrossRef]
48. Shijina, S.S.; Akbar, S.; Sajith, V. Graphene functionalized nano-encapsulated composite phase change material based nanofluid for battery cooling: An experimental investigation. *Appl. Therm. Eng.* **2025**, *259*, 124893. [CrossRef]
49. Sivashankar, M.; Selvam, C.; Suresh, S. Experimental study on the performance of low concentrated solar photovoltaic system with nano-enhanced phase change material encapsulated heat sink. *Appl. Therm. Eng.* **2025**, *262*, 125254. [CrossRef]
50. Sutheesh, P.M.; Thomas, R.; Bandaru, R. Battery thermal management systems by using DI water and PCF with Nano-encapsulated Tetradecan-1-ol for Lithium-ion batteries. *Int. Commun. Heat Mass Transf.* **2025**, *165*, 108992. [CrossRef]

51. Han, Y.; Wang, L.; Cao, K.; Zhou, J.; Zhu, Y.; Hou, Y.; Lu, Y. In Situ TEM Characterization and Modulation for Phase Engineering of Nanomaterials. *Chem. Rev.* **2023**, *123*, 14119–14184. [CrossRef]
52. He, Q.; Sheng, B.; Zhu, K.; Zhou, Y.; Qiao, S.; Wang, Z.; Song, L. Phase Engineering and Synchrotron-Based Study on Two-Dimensional Energy Nanomaterials. *Chem. Rev.* **2023**, *123*, 10750–10807. [CrossRef]
53. Liu, X.; Shan, J.; Cao, T.; Zhu, L.; Ma, J.; Wang, G.; Shi, Z.; Yang, Q.; Ma, M.; Liu, Z.; et al. On-device phase engineering. *Nat. Mater.* **2024**, *23*, 1363–1369. [CrossRef]
54. Zang, P.; Yu, C.; Zhang, R.; Yang, D.; Gai, S.; Liu, B.; Shen, R.; Yang, P.; Lin, J. Phase Engineered CuxS–Ag2S with Photothermoelectric Activity for Enhanced Multienzyme Activity and Dynamic Therapy. *Adv. Mater.* **2024**, *36*, 2400416. [CrossRef] [PubMed]
55. Yang, Z.; Ding, Y.; Chen, W.; Luo, S.; Cao, D.; Long, X.; Xie, L.; Zhou, X.; Cai, X.; Liu, K.; et al. Phase-Engineered Bi-RuO_2 Single-Atom Alloy Oxide Boosting Oxygen Evolution Electrocatalysis in Proton Exchange Membrane Water Electrolyzer. *Adv. Mater.* **2025**, *37*, 2417777. [CrossRef] [PubMed]
56. Çiçek, B. A numerical comparison of the thermal performances of nano-PCM heat sinks with Fe_3O_4, MgO, ZnO and xGNP nanoparticles: Key role of increased thermal conductivity. *Therm. Sci. Eng. Prog.* **2025**, *63*, 103712. [CrossRef]
57. Praveenkumar, N.; Lingadurai, K.; Ramkumar, T.; Bharathiraja, R. Characterization and thermophysical property evaluation of ceramic and metal oxide-based hybrid nanoparticles enhanced paraffin PCM. *J. Therm. Anal. Calorim.* **2025**, *150*, 3319–3334. [CrossRef]
58. Zhai, Z.; Zhu, J.; Cao, S.; Zhang, Y.; Van der Bruggen, B. Supramolecular Engineering of Metal–Organic Membranes with Metal-Support Interactions for Nanoconfined Synergistic Catalysis. *Small Methods* **2025**, 2500409. [CrossRef]
59. Karimipour, A.; Asiri, S.A.; Alfawaz, K.M.; Alogla, A.F.; Abu-Hamdeh, N.H.; Viet, P.H.H. The use of molecular dynamics method to evaluate the thermo-physical properties of Cu nanoparticles dispersed in Paraffin wax PCM. *J. Taiwan Inst. Chem. Eng.* **2024**, *165*, 105785. [CrossRef]
60. Geng, L.; Ali, A.B.M.; Babadoust, S.; Kumar, A.; Abdullaeva, B.; Hussein, R.A.; Salahshour, S.; Esmaeili, S. Modeling the influence of external heat flux on thermal characteristics of the silica aerogel/paraffin in a cylindrical atomic duct. *Case Stud. Therm. Eng.* **2025**, *65*, 105633. [CrossRef]
61. Mim, M.; Habib, K.; Farabi, S.N.; Zaed, M.A.; Saidur, R. Investigation of the thermophysical properties of PCMs with novel ionic liquid assisted nanocomposite for sustainable thermal energy storage application. *Case Stud. Therm. Eng.* **2025**, *70*, 106117. [CrossRef]
62. Liu, Y.; Basem, A.; Al-zahy, Y.M.A.; Singh, N.S.S.; Al-Bahrani, M.; Abduvalieva, D.; Salahshour, S.; Esmaeili, S. Molecular dynamics simulation of thermal behavior of paraffin/Cu nanoparticle PCM in a non-connected rotating ribbed tube. *Int. Commun. Heat Mass Transf.* **2025**, *165*, 109058. [CrossRef]
63. Sawaran Singh, N.S.; Hassan, W.H.; Thiab, R.F.; Al-zahy, Y.M.A.; Salahshour, S.; Hekmatifar, M. Effect of copper nanoparticle volume fraction on flow in a 3D lid-driven cavity with phase change materials using molecular dynamics simulation. *Case Stud. Chem. Environ. Eng.* **2025**, *11*, 101181. [CrossRef]
64. Cao, C.; Ali, A.B.M.; Hussein, Z.A.; Sawaran Singh, N.S.; Abdullaeva, B.; Zubair, A.; Salahshour, S.; Baghaei, S. Analysis of different phase change materials (PCMs) and wall material in a nano-circular space thermal energy storage (TES) system: A molecular dynamics approach. *Int. J. Therm. Sci.* **2025**, *215*, 109954. [CrossRef]
65. Huang, W.; Zhou, G. Molecular dynamics simulation of heat, mass and phonon transport performances of nanoparticle enhanced $Na_2SO_4 \cdot 10H_2O$. *J. Mol. Liq.* **2024**, *397*, 124157. [CrossRef]
66. Gao, Y.; Basem, A.; Mohammad Sajadi, S.; Jasim, D.J.; Nasajpour-Esfahani, N.; Salahshour, S.; Esmaeili, S.; Baghaei, S. The effect of initial pressure on the thermal behavior of the silica aerogel/PCM/CuO nanostructure inside a cylindrical duct using molecular dynamics simulation. *Case Stud. Therm. Eng.* **2024**, *54*, 104064. [CrossRef]
67. Yang, J.; Ali, A.B.M.; Al-zahy, Y.M.A.; Sawaran Singh, N.S.; Al-Bahrani, M.; Orlova, T.; Rahimi, M.; Salahshour, S.; Esmaeili, S. The effect of copper oxide nanoparticles on the thermal behavior of silica aerogel/paraffin as a phase change material in a cylindrical channel with molecular dynamics simulation. *Prog. Nucl. Energy* **2025**, *181*, 105645. [CrossRef]
68. Ru, Y.; Ali, A.B.M.; Qader, K.H.; Singh, N.S.S.; Jhala, R.; Soliyeva, M.; Salahshour, S.; Esmaeili, S. Investigating the effect of copper oxide nanoparticles radius on thermal behavior of silica aerogel/paraffin nanostructure using molecular dynamics simulation. *Int. Commun. Heat Mass Transf.* **2025**, *161*, 108547. [CrossRef]
69. An, Q.; Bagheritabar, M.; Basem, A.; Ghabra, A.A.; Li, Y.; Tang, M.; Sabri, L.S.; Sabetvand, R. The effect of size of copper oxide nanoparticles on the thermal behavior of silica aerogel/paraffin nanostructure in a duct using molecular dynamics simulation. *Case Stud. Therm. Eng.* **2024**, *60*, 104666. [CrossRef]
70. Yu, Y.; Liu, Y.; Chai, H.; Tian, H.; Wu, X.; Zhao, C. Nanoscale insight into the thermal properties of lauric acid and CuO based phase change material used for thermal energy storage. *J. Mol. Liq.* **2024**, *393*, 123630. [CrossRef]
71. Fang, M.; Cao, L.; Cao, Y. Optimization of thermophysical properties of molten salt-based date-occupied composites based on orthogonal tests. *J. Energy Storage* **2024**, *102*, 114183. [CrossRef]

72. Badreldin, A.; Bouhali, O.; Abdel-Wahab, A. Complimentary Computational Cues for Water Electrocatalysis: A DFT and ML Perspective. *Adv. Funct. Mater.* **2024**, *34*, 2312425. [CrossRef]
73. Rajabi, A.; Grotjahn, R.; Rappoport, D.; Furche, F. A DFT perspective on organometallic lanthanide chemistry. *Dalton Trans.* **2024**, *53*, 410–417. [CrossRef] [PubMed]
74. Chen, Z.; Zhang, J.; Deng, S.; Hou, M.; Zhang, X.; Jiang, Z.; Lai, N.-C. Morphology-controlled synthesis of Cu_2O encapsulated phase change materials: Photothermal conversion and storage performance in visible light regime. *Chem. Eng. J.* **2023**, *454*, 140089. [CrossRef]
75. Liang, S.; Wang, X.; Chen, L.; Qiu, X. Utilizing heterogeneity of lignin to diminish supercooling of phase change material nano-capsules with high latent heat. *J. Colloid Interface Sci.* **2025**, *683*, 833–840. [CrossRef]
76. Zhang, G.; Ren, S.; Dong, C.; Dong, W.; Du, Q.; Chen, X.; Li, A. Ni@graphite carbon synergistic reinforcement sites penetrated hierarchical porous carbon boosting PCMs encapsulation and solar-thermal energy storage. *Compos. Sci. Technol.* **2025**, *268*, 111228. [CrossRef]
77. Yao, Z.; Xie, J.; Fu, T.; Luo, Y.; Yang, X. One-pot preparation of phase change material employing nano-scaled resorcinol-furfural frameworks. *Chem. Eng. J.* **2024**, *484*, 149553. [CrossRef]
78. Tan, X.; Gu, X.; Nian, H.; Wang, X.; Li, J.; Wang, Q.; Wang, Z.; Zhao, Y.; Zhou, Y. Enhanced thermal performance of $NaCH_3COO{\cdot}3H_2O$-$Na_2S_2O_3{\cdot}5H_2O$ eutectic based composite phase change materials with hybrid dimensional carbon nanomaterials and modified lotus root starch. *J. Energy Storage* **2024**, *95*, 112418. [CrossRef]
79. Yuan, K.; Zhang, A.; Li, S.; Zhou, T.; Wang, Q.; Cao, W. Nanopore constrained thermal characteristics investigation of MIL-101 (Fe)/tetradecanol composite phase change materials. *Surf. Interfaces* **2025**, *60*, 106013. [CrossRef]
80. Wang, K.; Xue, Y.; Lin, J.; Yu, J.; Wang, Q.; Xie, Z.; Yu, H.; Qiu, X. ZIF-8 based microspheres with ordered mesopores and dual responsive surfaces. *Surf. Interfaces* **2023**, *38*, 102876. [CrossRef]
81. Zeng, X.; Zhu, X.; Sun, Y.; Hu, Y. Improving the thermal stability and operation speed of Sb_7Se_3 films via carbon nanolayers. *Appl. Surf. Sci.* **2024**, *651*, 159295. [CrossRef]
82. Xin, Y.-X.; Hu, D.; Li, J.-H.; Ge, Y.-X.; Wang, Y.-X. Incorporated surfaces and confined spaces of $Na_2HPO_4{\cdot}12H_2O$–Layered vermiculite nanosheets for phase change materials with enhanced thermal properties. *Appl. Surf. Sci.* **2024**, *675*, 160881. [CrossRef]
83. Kwon, M.S.; Jin, X.; Kim, Y.C.; Hu, J.W. Development of microencapsulated PCM concrete with improved strength and long-term thermal performance using MWCNTs. *Constr. Build. Mater.* **2024**, *442*, 137609. [CrossRef]
84. Yeşilata, B.; Bayram, M.; Ustaoğlu, A.; Kurşuncu, B.; Hekimoğlu, G.; Sarı, A.; Çıkman, İ.Ü.; Gencel, O.; Ozbakkaloglu, T. Effects of Cavity-Shapes in 3D printed PCM encapsulation plates on sustainable thermal energy efficiency in buildings. *Therm. Sci. Eng. Prog.* **2025**, *62*, 103570. [CrossRef]
85. Bonifacio, C.S.; Yu, Y.; Ray, M.L.; Skowronski, M.; Fischione, P. TEM Preparation and Characterization of a GeTe-based Phase Change Memory Device at Partial SET Mode. *Microsc. Microanal.* **2024**, *30*, ozae044-607. [CrossRef]
86. Karimi, Y.; Solaimany Nazar, A.R.; Molla-Abbasi, P. Synthesis, characterization and application of a magnetic nanoencapsulated PCM in enhancing the natural convection in a cube cavity. *Therm. Sci. Eng. Prog.* **2024**, *47*, 102342. [CrossRef]
87. Ennamri, A.; Bencaid, J.; Draoui, K.; Ouarga, A.; Oualid, H.A. Development of a new kaolinite/phase change material (PCM) composite for latent heat thermal energy storage in building applications. *Mater. Sci. Eng. B* **2025**, *319*, 118366. [CrossRef]
88. Hassan, E.A.; Tony, M.A.; Awad, M.M. Thermal Energy Storage Using Hybrid Nanofluid Phase Change Material (PCM) Based on Waste Sludge Incorp Rated ZnO/α-Fe_2O_3. *Nanomaterials* **2024**, *14*, 604. [CrossRef]
89. Jiang, D.; Chen, P.; Liu, J.; Xu, Y. Preparation and performance study of modified diatomite based PCM for construction. *Green Mater.* **2024**, 1–13. [CrossRef]
90. Vignesh, T.; Selvakumar, D.; Madhankumar, S. Drying kinetics, energy, colour and FTIR spectroscopy analysis on indirect solar dryer with paraffin wax and glass pieces as thermal storage material. *Sol. Energy* **2024**, *282*, 112925. [CrossRef]
91. Gao, M.; Zhao, S.; Yang, H.; Wu, X.; Xiao, Y. An Analysis of the Influence of DSC Parameters on the Measurement of the Thermal Properties of Phase-Change Material. *Materials* **2024**, *17*, 5689. [CrossRef]
92. Laasri, I.A.; Charai, M.; Es-sakali, N.; Mghazli, M.O.; Outzourhit, A. Evaluating passive PCM performance in building envelopes for semi-arid climate: Experimental and numerical insights on hysteresis, sub-cooling, and energy savings. *J. Build. Eng.* **2024**, *98*, 111161. [CrossRef]
93. El Majd, A.; Sair, S.; Ousaleh, H.A.; Bouhaj, Y.; Belouaggadia, N.; Younsi, Z.; El Bouari, A. Advancing tent thermoregulation: Integrating shape-stabilized PCM into fabric design. *J. Energy Storage* **2024**, *95*, 112681. [CrossRef]
94. Naqvi, S.N.R.; Haider, M.Z.; Jin, X.; Hu, J.W. Investigation of thermal and mechanical performance of composite PCM mortar incorporated with graphene nanoplatelets. *Constr. Build. Mater.* **2025**, *470*, 140576. [CrossRef]
95. Ayyagari, V.; Shooshtari, A.; Ohadi, M. Glauber's Salt Composites for HVAC Applications: A Study on the Use of the T-History Method with a Modified Data Evaluation Methodology. *Materials* **2025**, *18*, 2998. [CrossRef] [PubMed]
96. Solé, A.; Miró, L.; Barreneche, C.; Martorell, I.; Cabeza, L.F. Review of the T-history method to determine thermophysical properties of phase change materials (PCM). *Renew. Sustain. Energy Rev.* **2013**, *26*, 425–436. [CrossRef]

97. Wang, M.; Wang, J. Flow boiling of nanofluids in microchannel heat exchangers: A critical review. *Therm. Sci. Eng. Prog.* **2024**, *55*, 102930. [CrossRef]
98. Behseresht, S.; Park, Y.H. Additive Manufacturing of Composite Polymers: Thermomechanical FEA and Experimental Study. *Materials* **2024**, *17*, 1912. [CrossRef]
99. Smolnicki, M.; Lesiuk, G.; Duda, S.; de Jesus, A.M.P. A Review on Finite-Element Simulation of Fibre Metal Laminates. *Arch. Comput. Methods Eng.* **2023**, *30*, 749–763. [CrossRef]
100. Gürsoy, E. Melting and energy storage performance enhancement of rectangular cavity with metal foam by nano-PCM and recessed/protruding dimpled fin wall. *J. Energy Storage* **2025**, *119*, 116327. [CrossRef]
101. Hekmat, M.H.; Saharkhiz, S. Impact of helically coiled shell and tube on melting and solidification of PCMs in thermal energy storage systems: A three-dimensional parametric study. *J. Energy Storage* **2025**, *108*, 115172. [CrossRef]
102. Dora, S.; Kuznik, F.; Mini, K.M. A novel PCM-based foam concrete for heat transfer in buildings -Experimental developments and simulation modelling. *J. Energy Storage* **2025**, *105*, 114625. [CrossRef]
103. Yang, B.; Xie, L.; Cao, Y.; Yu, X. The role of porosity gradient distribution on the heat transfer characteristics of copper foam/paraffin composite phase change material. *J. Energy Storage* **2025**, *127*, 117157. [CrossRef]
104. Zhao, W.; Yu, G.; Li, S.; Liu, Z.; Wu, L. Rate capability and Ragone plots for thermal management multifunctional structure designing. *Int. J. Mech. Sci.* **2023**, *252*, 108367. [CrossRef]
105. Sun, H.; Li, M.; Li, T.; Zhao, J.; Du, Q.; Li, B.; Sun, D. Regulation of carbonized cellulose nanofiber pore structure by artificially cultured diatom frustules for leakage-proof phase change composites. *Chem. Eng. J.* **2025**, *504*, 158482. [CrossRef]
106. Saleh, H. Heat transfer enhancement in a nano encapsulated PCM-water filled square cavity with flexible fin. *J. Energy Storage* **2024**, *85*, 111121. [CrossRef]
107. Egami, R.H.; Almalki, A.S.; Alharbi, I.S. Simulation of freezing process of PCM in existence of nano-sized additives within storage tank. *J. Therm. Anal. Calorim.* **2024**, *149*, 4575–4586. [CrossRef]
108. Tominaga, Y. CFD simulations of turbulent flow and dispersion in built environment: A perspective review. *J. Wind Eng. Ind. Aerodyn.* **2024**, *249*, 105741. [CrossRef]
109. Wang, M.; Ju, H.; Wu, J.; Qiu, H.; Liu, K.; Tian, W.; Su, G.H. A review of CFD studies on thermal hydraulic analysis of coolant flow through fuel rod bundles in nuclear reactor. *Prog. Nucl. Energy* **2024**, *171*, 105175. [CrossRef]
110. Olivares-Robles, M.A.; Enciso-Montes de Oca, O.Y.; Vargas-Almeida, A. Optimizing the transient response of an annular thermoelectric cooler: PCM and nanofluid synergy. *J. Energy Storage* **2025**, *115*, 115950. [CrossRef]
111. Benyahia, I.; Al-Ghamdi, M.F.; Abderrahmane, A.; Younis, O.; Laouedj, S.; Guedri, K.; Alahmer, A. Comprehensive thermal analysis of a nano-enhanced PCM in a finned latent heat storage system. *Int. Commun. Heat Mass Transf.* **2025**, *165*, 109106. [CrossRef]
112. Bouzennada, T.; Abderrahmane, A.; Aich, W.; Younis, O.; Ben Ali, N.; Kolsi, L. Heat transfer and fluid flow in nano-encapsulated PCM-filled undulated cavity. *Ain Shams Eng. J.* **2024**, *15*, 102669. [CrossRef]
113. Gholami, A.; Parach, K.; Jafari, B. Numerical analysis of a photovoltaic panel containing hybrid nanoparticles integrated with PCM in the presence of fixed fins. *Case Stud. Therm. Eng.* **2025**, *70*, 106098. [CrossRef]
114. Nandi, A.; Biswas, N. Enhanced melting dynamics of phase change material (PCM) based energy storage system combining modified fin and nanoparticles under solar irradiation. *Int. J. Numer. Methods Heat Fluid Flow* **2025**, *35*, 2104–2143. [CrossRef]
115. Shaik, S.A.; Nigam, P.K.; Gugulothu, S.K. Advanced fin designs for improved thermal management in PCM-based latent heat storage systems. *Appl. Therm. Eng.* **2025**, *272*, 126337. [CrossRef]
116. Waqas, H.; Hussain, M.; Al-Mdallal, Q.M.; Ahammad, N.A.; Elseesy, I.E. The impact of nano-infused phase change materials and blossom-shaped fins on thermal energy storage. *Case Stud. Therm. Eng.* **2025**, *65*, 105623. [CrossRef]
117. Mahdavi, A.; Niloofari, P.; Gorji-Bandpy, M.; Mahmoudi, A. Numerical simulation of a PVT-PCM system by altering fluid tube positioning adding nanoparticles and embedding a porous medium. *Alex. Eng. J.* **2025**, *115*, 30–46. [CrossRef]
118. Alam, M.T.; Garg, V.; Soni, V.; Gupta, A.K. Effect of enclosure design with composite/nano-enhanced/dual phase change material on melting response of latent heat storage systems. *Chem. Eng. Res. Des.* **2025**, *214*, 125–143. [CrossRef]
119. Kiyak, B.; Biswas, N.; Öztop, H.F.; Selimefendigil, F. Geometry curvature influence on melting and solidification performance in nano particle added phase change material to storage energy. *J. Energy Storage* **2025**, *117*, 116172. [CrossRef]
120. Amin, M.; Putra, N.; Rizal, T.A.; Umar, H.; Ginting, S.F.; Amir, F.; Kusuma, M.H. Enhanced tubular solar still performance using nano beeswax/graphene phase change materials and parabolic trough collectors. *J. Energy Storage* **2025**, *124*, 116884. [CrossRef]
121. Singh, A.P.; Tiwari, S.; Sinhmar, H.; Pal, G.; Pandey, A.K. Experimental study on PCM (OM-37) enhanced with nanoparticles for improved heat retention in solar ponds. *J. Energy Storage* **2025**, *123*, 116760. [CrossRef]
122. Emara, K.; Abd-Elgawad, A.M.M.M.; Emara, A. Effect of nanofluids-PCM heat exchanging on engine downsizing and heat transfer enhancement via the heat engine's cooling system: A novel saving tactic. *J. Energy Storage* **2025**, *117*, 115815. [CrossRef]

123. Al-Karboly, A.M.O.; Ibrahim, A.; Fazlizan, A.; Sopian, K.; Al-Aasam, A.B.; Ishak, M.A.A.B.; Al-Waeli, A.H.A.; Elmnifi, M. Experimental evaluation of a photovoltaic thermal collector using twisted tape absorber with nano-enhanced phase change material for thermal storage. *J. Energy Storage* **2025**, *109*, 115122. [CrossRef]
124. Kamrava, M.; Fazilati, M.A.; Toghraie, D. Investigating the use of nano-enhanced phase change material in floor heating system: A numerical approach. *Int. Commun. Heat Mass Transf.* **2025**, *164*, 108962. [CrossRef]
125. Gür, M.; Gürgenç, E.; Coşanay, H.; Öztop, H.F. Solar-assisted radiant heating system with nano-B4C enhanced PCM for nearly zero energy buildings. *Case Stud. Therm. Eng.* **2025**, *65*, 105544. [CrossRef]
126. Sathishkumar, A.; Cheralathan, M. Charging and discharging processes of low capacity nano-PCM based cool thermal energy storage system: An experimental study. *Energy* **2023**, *263*, 125700. [CrossRef]
127. Bassam, A.M.; Sopian, K.; Ibrahim, A.; Al-Aasam, A.B.; Dayer, M. Experimental analysis of photovoltaic thermal collector (PVT) with nano PCM and micro-fins tube counterclockwise twisted tape nanofluid. *Case Stud. Therm. Eng.* **2023**, *45*, 102883. [CrossRef]
128. Bassam, A.M.; Sopian, K.; Ibrahim, A.; Fauzan, M.F.; Al-Aasam, A.B.; Abusaibaa, G.Y. Experimental analysis for the photovoltaic thermal collector (PVT) with nano PCM and micro-fins tube nanofluid. *Case Stud. Therm. Eng.* **2023**, *41*, 102579. [CrossRef]
129. Kibria, M.G.; Mohtasim, M.S.; Paul, U.K.; Das, B.K.; Saidur, R. Impact of hybrid nano PCM (paraffin wax with Al_2O_3 and ZnO nanoparticles) on photovoltaic thermal system: Energy, exergy, exergoeconomic and enviroeconomic analysis. *J. Clean. Prod.* **2024**, *436*, 140577. [CrossRef]
130. Bharathiraja, R.; Ramkumar, T.; Selvakumar, M.; Sasikumar, K. Experimental and numerical analysis of hybrid nano-enhanced phase change material (PCM) based flat plate solar collector. *J. Energy Storage* **2024**, *96*, 112649. [CrossRef]
131. Mousavi, S.M.; Khanmohammadi, F.; Rabienataj Darzi, A.A. Magnetic influence on phase change materials for optimized thermal energy storage: A comprehensive review and prospective insights. *J. Energy Storage* **2024**, *89*, 111625. [CrossRef]
132. Izadi, M.; Sheremet, M.; Hajjar, A.; Galal, A.M.; Mahariq, I.; Jarad, F.; Ben Hamida, M.B. Numerical investigation of magneto-thermal-convection impact on phase change phenomenon of Nano-PCM within a hexagonal shaped thermal energy storage. *Appl. Therm. Eng.* **2023**, *223*, 119984. [CrossRef]
133. Hassan, A.M.; Alomari, M.A.; Alajmi, A.; Sadeq, A.M.; Alqurashi, F.; Flayyih, M.A. Enhanced natural convection in a U-shaped baffled cavity: Synergistic effects of magnetic fields and wall oscillations on Nano-encapsulated PCM. *Int. Commun. Heat Mass Transf.* **2025**, *165*, 109051. [CrossRef]
134. Younis, O.; Laidoudi, H.; Abderrahmane, A.; Belazreg, A.; Qasem, N.A.A.; Homod, R.Z.; Yacine, k.; Rawa, M.; Hassan, A.M. Thermal pattern of nano-encapsulated PCM in a lid-driven cavity with presence of a heated body, magnetic field and limited permeability. *Case Stud. Therm. Eng.* **2023**, *50*, 103469. [CrossRef]
135. Selimefendigil, F.; Oztop, H.F. Effects of location of nano-enhanced PCM-packed bed on the process of heat transfer and phase transition in a nonuniform magnetic field. *Numer. Heat Transf. Part A Appl.* **2024**, 1–21. [CrossRef]
136. Selimefendigil, F.; Öztop, H.F. Multijet impingement heat transfer under the combined effects of encapsulated-PCM and inclined magnetic field during nanoliquid convection. *Int. J. Heat Mass Transf.* **2023**, *203*, 123764. [CrossRef]
137. Selimefendigil, F.; Oztop, H.F. Convection and phase change in a lid-driven trapezoidal vented cavity with encapsulated PCM under non-uniform magnetic field by using ternary nanofluid. *Therm. Sci. Eng. Prog.* **2024**, *48*, 102424. [CrossRef]
138. Nguyen, L.M.Q.; Alshuraiaan, B.; Hajjar, A.; Izadi, M.; El Idi, M.M. Assessment of the thermal resistance of novel roof structures incorporating nano-Phase Change Materials capsules under the influence of an external magnetic field. *J. Build. Eng.* **2023**, *79*, 107851. [CrossRef]
139. Lu, B.; Zhang, Y.; Xiao, J.; Hu, M.; Niu, Y.; Luo, M.; Zhu, J.; Zhang, J. Experimental investigation of the effect of rotating magnetic field on the melting performance enhancement of paraffin/nano-Fe3O4 composite phase change material. *J. Energy Storage* **2024**, *83*, 110751. [CrossRef]
140. Li, H.; Zhuang, Y.; Feng, J.-C. Multi-scale experimental analysis on the coupled effects of ultrasonic field and magnetic field on the melting and energy storage performances for hybrid nano-enhanced phase change materials. *J. Energy Storage* **2024**, *84*, 110801. [CrossRef]
141. Zhuang, Y.; Li, H.; Xu, W.; Huang, S.-M. Experimental study on the melting performance of magnetic NEPCMs embedded in metal foam subjected to a non-uniform magnetic field. *Sol. Energy Mater. Sol. Cells* **2023**, *250*, 112077. [CrossRef]
142. Farahani, S.D.; Farahani, A.D.; Mamoei, A.J.; Yan, W.-M. Enhancement of phase change material melting using nanoparticles and magnetic field in the thermal energy storage system with strip fins. *J. Energy Storage* **2023**, *57*, 106282. [CrossRef]
143. Zhou, Y.; Zhang, W.; Ma, E.; Deringer, V.L. Device-scale atomistic modelling of phase-change memory materials. *Nat. Electron.* **2023**, *6*, 746–754. [CrossRef]
144. Taheri, M.; Pourfayaz, F.; Hemmati, S. A highly accurate model for prediction of thermal conductivity of carbon-based nano-enhanced PCMs using an artificial neural network. *Energy Rep.* **2023**, *10*, 1249–1258. [CrossRef]
145. Sharma, A.; Singh, P.K.; Makki, E.; Giri, J.; Sathish, T. A comprehensive review of critical analysis of biodegradable waste PCM for thermal energy storage systems using machine learning and deep learning to predict dynamic behavior. *Heliyon* **2024**, *10*, e25800. [CrossRef] [PubMed]

146. Shakibi, H.; Shokri, A.; Sobhani, B.; Yari, M. Numerical analysis and optimization of a novel photovoltaic thermal solar unit improved by Nano-PCM as an energy storage media and finned collector. *Renew. Sustain. Energy Rev.* **2023**, *179*, 113230. [CrossRef]
147. Aly, A.M.; Alsedais, N. Heat and mass transfer of NEPCM in a wavy porous cavity with variable hot and high-concentration zones: A study using ISPH and XGBoost models. *Int. Commun. Heat Mass Transf.* **2025**, *160*, 108383. [CrossRef]
148. Abdolahimoghadam, M.; Rahimi, M. New hybrid nano-and bio-based phase change material containing graphene-copper particles hosting beeswax-coconut oil for solar thermal energy storage: Predictive modeling and evaluation using machine learning. *Energy* **2024**, *307*, 132604. [CrossRef]
149. Abdolahimoghadam, M.; Rahimi, M. Experimental, numerical, and machine learning study of vertical thermal energy storage filling with novel hybrid nano-and bio-based phase change material. *J. Energy Storage* **2025**, *106*, 114815. [CrossRef]
150. Gao, Y.; Shigidi, I.M.T.A.; Ali, M.A.; Homod, R.Z.; Safaei, M.R. Thermophysical properties prediction of carbon-based nano-enhanced phase change material's using various machine learning methods. *J. Taiwan Inst. Chem. Eng.* **2023**, *148*, 104662. [CrossRef]
151. Ghasemi, H.; Sheikhzadeh, G.A.; Fattahi, A. Numerical Simulation and ANN Prediction of Nano-Encapsulated PCM Slurry in a Microchannel: A Thermodynamic Analysis. *Arab. J. Sci. Eng.* **2025**. [CrossRef]
152. Kiaghadi, M.; Keshvarinia, M.; Boora, F.M.; Mousavi, S.M. Machine learning applications for predicting liquid fraction in a PV system with NEPCM and fins. *Case Stud. Therm. Eng.* **2024**, *61*, 104819. [CrossRef]
153. Kiaghadi, M.; Sheikholeslami, M.; Alinia, A.M.; Boora, F.M. Predicting the performance of a photovoltaic unit via machine learning methods in the existence of finned thermal storage unit. *J. Energy Storage* **2024**, *90*, 111766. [CrossRef]
154. Yang, Y.; Wang, Z.; Ayed, H.; Alhoee, J. Incorporating nickel foam with nano-encapsulated phase change material and water emulsion for battery thermal management: Coupling CFD and machine learning. *Case Stud. Therm. Eng.* **2024**, *60*, 104672. [CrossRef]
155. Xu, S.; Basem, A.; Al-Asadi, H.A.; Chaturvedi, R.; Daminova, G.; Fouad, Y.; Jasim, D.J.; Alhoee, J. Employing deep learning for predicting the thermal properties of water and nano-encapsulated phase change material. *Int. J. Low-Carbon Technol.* **2024**, *19*, 1453–1459. [CrossRef]
156. Salari, A.; Ahmadi, R.; Vafadaran, M.S.; Shakibi, H.; Sardarabadi, M. Predicting the performance of a heat sink utilized with an energy storage unit using machine learning approach. *J. Energy Storage* **2024**, *83*, 110470. [CrossRef]
157. Khadem, Z.; Salari, A.; Naghdbishi, A.; Shakibi, H.; Sardarabadi, M. Parametric analysis of a PCM-based heat sink for electronic device thermal management. *J. Energy Storage* **2023**, *74*, 109118. [CrossRef]
158. Fini, A.T.; Fattahi, A.; Musavi, S. Machine learning prediction and multiobjective optimization for cooling enhancement of a plate battery using the chaotic water-microencapsulated PCM fluid flows. *J. Taiwan Inst. Chem. Eng.* **2023**, *148*, 104680. [CrossRef]
159. Coletti, K.; Romeo, R.C.; Davis, R.B. Bayesian backcalculation of pavement properties using parallel transitional Markov chain Monte Carlo. *Comput.-Aided Civ. Infrastruct. Eng.* **2024**, *39*, 1911–1927. [CrossRef]
160. Chen, Z.; Mak, S.; Wu, C.F.J. A Hierarchical Expected Improvement Method for Bayesian Optimization. *J. Am. Stat. Assoc.* **2024**, *119*, 1619–1632. [CrossRef]
161. Alazwari, M.A.; Algarni, M.; Safaei, M.R. Effects of various types of nanomaterials on PCM melting process in a thermal energy storage system for solar cooling application using CFD and MCMC methods. *Int. J. Heat Mass Transf.* **2022**, *195*, 123204. [CrossRef]
162. Goodarzi, M.; Elkotb, M.A.; Alanazi, A.K.; Abo-Dief, H.M.; Mansir, I.B.; Tirth, V.; Gamaoun, F. Applying Bayesian Markov chain Monte Carlo (MCMC) modeling to predict the melting behavior of phase change materials. *J. Energy Storage* **2022**, *45*, 103570. [CrossRef]
163. Wang, Z.; Bu, S.; Wen, J.; Huang, C. A comprehensive review on uncertainty modeling methods in modern power systems. *Int. J. Electr. Power Energy Syst.* **2025**, *166*, 110534. [CrossRef]
164. Azarhoosh, Z.; Ilchi Ghazaan, M. A Review of Recent Advances in Surrogate Models for Uncertainty Quantification of High-Dimensional Engineering Applications. *Comput. Methods Appl. Mech. Eng.* **2025**, *433*, 117508. [CrossRef]
165. Al-Aasam, A.B.; Ibrahim, A.; Sopian, K.; Abdulsahib, M.B.; Dayer, M. Nanofluid-based photovoltaic thermal solar collector with nanoparticle-enhanced phase change material (Nano-PCM) and twisted absorber tubes. *Case Stud. Therm. Eng.* **2023**, *49*, 103299. [CrossRef]
166. Daneshazarian, R.; Eslami, R.; Azizi, N.; Zarrin, H.; Berardi, U. Performance evaluation of a novel nano-enhanced phase change material for thermal energy storage applications. *J. Energy Storage* **2023**, *74*, 109376. [CrossRef]
167. Gür, M.; Gürgenç, E.; Coşanay, H.; Öztop, H.F. Novel nano-Y_2O_3/myristic acid nanocomposite PCM for cooling performances of electronic device with various fin designs. *J. Energy Storage* **2024**, *100*, 113646. [CrossRef]
168. Venkatesh, R.; Karthik, K.; Vinayagam, M.; Verma, A.; Chaturvedi, R.; Soudagar, M.E.M.; Bhooshanam, N.N.; Al Obaid, S.; Alharbi, S.A. Enhancement of solar cooking performance by utilizing hybrid SiC/Ag featured nano-PCM heat exchanger integrated with parabolic trough collector. *J. Therm. Anal. Calorim.* **2024**, *149*, 14389–14402. [CrossRef]

169. GaneshKumar, P.; Vigneswaran, V.S.; Murugan, P.; Cheralathan, M.; Velraj, R.; Kim, S.C.; Ramkumar, V. Exploring the thermal performance of a solar air heater with a V-corrugated and shot-blasted absorber plate comprising nano-enhanced phase change materials. *J. Energy Storage* **2024**, *77*, 109955. [CrossRef]
170. Osman, A.I.; Fang, B.; Zhang, Y.; Liu, Y.; Yu, J.; Farghali, M.; Rashwan, A.K.; Chen, Z.; Chen, L.; Ihara, I.; et al. Life cycle assessment and techno-economic analysis of sustainable bioenergy production: A review. *Environ. Chem. Lett.* **2024**, *22*, 1115–1154. [CrossRef]
171. Saez, R.; Boer, D.; Shobo, A.B.; Vallès, M. Techno-economic analysis of residential rooftop photovoltaics in Spain. *Renew. Sustain. Energy Rev.* **2023**, *188*, 113788. [CrossRef]
172. Ma, C.; Van Coile, R.; Gernay, T. Fire protection costs in composite buildings for cost-benefit analysis of fire designs. *J. Constr. Steel Res.* **2024**, *215*, 108517. [CrossRef]
173. Samat, N.; Goh, K.H.; See, K.F. Review of the application of cost–benefit analysis to the development of production systems in aquaculture. *Aquaculture* **2024**, *587*, 740816. [CrossRef]
174. Hekrle, M.; Liberalesso, T.; Macháč, J.; Matos Silva, C. The economic value of green roofs: A case study using different cost–benefit analysis approaches. *J. Clean. Prod.* **2023**, *413*, 137531. [CrossRef]
175. Dong, Z.; Bian, Z.; Jin, W.; Guo, X.; Zhang, Y.; Liu, X.; Wang, C.; Guan, D. An integrated approach to prioritizing ecological restoration of abandoned mine lands based on cost-benefit analysis. *Sci. Total Environ.* **2024**, *924*, 171579. [CrossRef]
176. Sharshir, S.W.; Abdo, M.R.; Yusuf, K.; El-Naggar, A.A.; Joseph, A.; Ismail, M.; Elsaid, A.M.; El-Samadony, M.O.A.; Abdelfatah, M.; El-Shaer, A.; et al. Thermo-economic and environmental evaluation of thin film evaporation using novel metal-organic frameworks to enhance solar desalination performance. *Process Saf. Environ. Prot.* **2025**, *199*, 107223. [CrossRef]
177. Rasaiah, N.; Eugine, R.; Manickam, R. Efficiency, productivity and economic analysis of polystyrene foam–insulated conventional and modified double-slope solar still using nanofluids. *Environ. Sci. Pollut. Res.* **2025**, *32*, 12713–12742. [CrossRef]
178. Kumar, K.; Sarkar, J.; Mondal, S.S. Energy, exergy, and economic evaluations of various cylindrical lithium-ion battery thermal management systems. *Int. Commun. Heat Mass Transf.* **2025**, *165*, 109007. [CrossRef]
179. Gürbüz, E.Y.; Şahinkesen, İ.; Tuncer, A.D.; Güler, O.V.; Keçebaş, A.; Georgiev, A.G. Experimental investigation of a baffled photovoltaic-thermal air collector with SiC nano-embedded thermal paste: A comparative study. *Renew. Energy* **2025**, *244*, 122649. [CrossRef]
180. Mohtasim, M.S.; Kibria, M.G.; Pranto, M.M.H.; Das, B.K. Hybrid PVT integrated pyramid solar still: 11E, sustainability, and sustainable development goals assessment. *Renew. Energy* **2025**, *246*, 122914. [CrossRef]
181. Singh, V.K.; Kumar, D. An experimental investigation and thermo-economic performance analysis of solar desalination system by using nano-enhanced PCM. *Mater. Today Sustain.* **2024**, *27*, 100884. [CrossRef]
182. Anika, U.A.; Kibria, M.G.; Kanka, S.D.; Mohtasim, M.S.; Paul, U.K.; Das, B.K. Exergy, exergo-economic, environmental and sustainability analysis of pyramid solar still integrated hybrid nano-PCM, black sand, and sponge. *Sol. Energy* **2024**, *274*, 112559. [CrossRef]
183. Vaziri Rad, M.A.; Rousta, M.; Khanalizadeh, A.; Kouravand, A.; Akbari, M.; Mousavi, S.; Razi Astaraei, F.; Sadeghitabar, E.; Yan, W.-M.; Kasaeian, A. Critical analysis of enhanced photovoltaic thermal systems: A comparative experimental study of PCM, TEG, and nanofluid applications. *Energy Convers. Manag.* **2024**, *314*, 118712. [CrossRef]
184. Essa, F.A.; Alawee, W.H.; Abdullah, A.S.; Mohammed, S.A.; Basem, A.; Majdi, H.S.; Omara, Z.M. Enhancing water evaporation rate in hemispherical solar distillers through innovative modifications and Nano-PCM integration. *Sol. Energy* **2024**, *271*, 112453. [CrossRef]
185. Paul, U.K.; Mohtasim, M.S.; Kibria, M.G.; Das, B.K. Nano-material based composite phase change materials and nanofluid for solar thermal energy storage applications: Featuring numerical and experimental approaches. *J. Energy Storage* **2024**, *98*, 113032. [CrossRef]
186. Elamy, M.I.; Mohammed, S.A.; Basem, A.; Alawee, W.H.; Abdullah, A.S.; Majdi, H.S.; Omara, Z.M.; Essa, F.A. Optimizing cord pyramid solar distillers: A comprehensive study on square baffles, reflectors, and phase transition materials. *Case Stud. Therm. Eng.* **2024**, *63*, 105304. [CrossRef]
187. Attia, M.E.H.; Abdelgaied, M.; Harby, K. New graphite fins efficacy on conical solar distiller performance: Experimental study with thermal, exergy, economic, and sustainability analysis. *J. Water Process Eng.* **2024**, *64*, 105652. [CrossRef]
188. El-Gazar, E.F.; Yousef, M.S.; Elshaer, A.M.; Khattab, M.A.; Mouneer, T.A.; Hawwash, A.A. Enhancing solar still performance with hybrid nanofluid: A comprehensive assessment of energy, exergy, economics, and environmental impact using a novel fractional model. *Environ. Dev. Sustain.* **2024**, 1–28. [CrossRef]
189. van Daalen, K.R.; Jung, L.; Dada, S.; Othman, R.; Barrios-Ruiz, A.; Malolos, G.Z.; Wu, K.T.; Garza-Salas, A.; El-Gamal, S.; Ezzine, T.; et al. Bridging the gender, climate, and health gap: The road to COP29. *Lancet Planet Health* **2024**, *8*, e1088–e1105. [CrossRef]
190. Fearnside, P.M.; Filho, W.L. COP 30: Brazilian policies must change. *Science* **2025**, *387*, 1237. [CrossRef]
191. Tilsted, J.P.; Newell, P. Synthetic transitions: The political economy of fossil fuel as feedstock. *Rev. Int. Political Econ.* **2025**, *32*, 1214–1238. [CrossRef]

192. Adom, P.K. Global energy efficiency transition tendencies: Development phenomenon or not? *Energy Strategy Rev.* **2024**, *55*, 101524. [CrossRef]
193. Shannak, S.d.; Cochrane, L.; Bobarykina, D. Strategic analysis of metal dependency in the transition to low-carbon energy: A critical examination of nickel, cobalt, lithium, graphite, and copper scarcity using IEA future scenarios. *Energy Res. Soc. Sci.* **2024**, *118*, 103773. [CrossRef]
194. Suárez-Cuesta, D.; Latorre, M.C. Governance and policy implications of the Inflation Reduction Act: A European perspective. *Glob. Policy* **2024**, *15*, 37–43. [CrossRef]
195. Rizos, V.; Urban, P. Barriers and policy challenges in developing circularity approaches in the EU battery sector: An assessment. *Resour. Conserv. Recycl.* **2024**, *209*, 107800. [CrossRef]
196. Sabyrbekov, R.; Overland, I. Small and large friends of the EU's carbon border adjustment mechanism: Which non-EU countries are likely to support it? *Energy Strategy Rev.* **2024**, *51*, 101303. [CrossRef]
197. Götz, V.; Harnesk, D. Transnational contestation for local communities within the formation of the European Union's Critical Raw Materials Act—A critical appraisal. *Environ. Politics* **2025**, 1–27. [CrossRef]
198. Froidevaux, J.S.P.; Le Viol, I.; Barré, K.; Bas, Y.; Kerbiriou, C. A modeling framework for biodiversity assessment in renewable energy development: A case study on European bats and wind turbines. *Renew. Sustain. Energy Rev.* **2025**, *211*, 115323. [CrossRef]
199. Bang, G. The U.S. Inflation Reduction Act: Climate policy as economic crisis response. *Environ. Politics* **2025**, 1–22. [CrossRef]
200. Sigman, H. Climate Change Adaptation in Government Decisions: Empirical Evidence from Superfund Remedies. *Land Econ.* **2025**, *101*, 18. [CrossRef]
201. Chen, H.; Niu, D.; Gao, Y. Research on the impact of energy transition policies on green total factor productivity of Chinese high-energy-consuming enterprises. *Energy* **2025**, *319*, 135066. [CrossRef]
202. Xinhua. China Unveils Draft of Its First-Ever Environmental Code. Available online: http://english.scio.gov.cn/in-depth/2025-04/28/content_117848751.html (accessed on 1 May 2025).
203. Jindal, A.; Puri, S.; Shrimali, G. Designing a prospective carbon trading market in India: Key properties, enabling features and linkages. *Appl. Energy* **2025**, *386*, 125595. [CrossRef]
204. Ha-Duong, M. Power system planning in the energy transition era: The case of Vietnam's power development plan 8. *Clim. Policy* **2025**, *25*, 562–577. [CrossRef]
205. Paulino de Azevedo, J.H.; Pradelle, F.; Botelho, V.; Torres Serra, E.; Nohra Chaar Pradelle, R.; Leal Braga, S. An integrated geospatial model for evaluating offshore wind-to-hydrogen technical and economic production potential in Brazil. *Int. J. Hydrogen Energy* **2025**, *100*, 800–815. [CrossRef]
206. Uratani, J.M.; Evensen, D.; Sovacool, B.K.; Griffiths, S. Benchmarking and tailoring electric vehicle policies to stimulate adoption. *Energy Res. Soc. Sci.* **2025**, *125*, 104074. [CrossRef]